NOLAN Project
Resistivity/IP Survey: Phase II

Dawson Mining District
NTS: 116C/01; 116C/02; 115N/16

Work Performed On: June 11th – June 25th, 2017 and
July 10th – July 21st, 2017

FOR:

White Gold Corp.
100 University Avenue, 8th Floor
Toronto, Ontario, Canada M5J 2Y1
(800) 564 6253

BY:
Jen Hanlon, M.Sc., GIT
GroundTruth Exploration Inc.
BOX 70, Dawson City, YT.

Date: October 24th, 2017
Table of Contents

Table of Figures

Table of Appendix Figures

1.0 Introduction

White Gold Corporation (WGO) headquartered in Toronto, ON commissioned GroundTruth Exploration Inc. (GroundTruth) headquartered in Dawson City, YT to complete high resolution resistivity and induced polarization (RES/IP) surveys on four

subproperties on the Nolan (NOL) property during the 2017 field season. These properties are the Cali, Nine Mile-NW, Nine Mile-SE, and Boucher.

The purpose of the RES/IP survey is to identify geological structure and delineate extent of mineralized zones that are indicated by soil anomalies. This report details the results of the RES/IP surveys. Additional surveying and interpretation is left to WGO's discretion.

Figure 1 shows an overview of the proposed RES/IP grid lines to be completed within the Nolan property during the 2017 field season. Note that there are 12 lines at the Cali, 8 lines at Nine Mile-NW, 5 lines at Nine Mile-SE, and 7 lines at Boucher. Maps of the completed grids are shown in Figures 2, 15, 21, and 29, respectively.

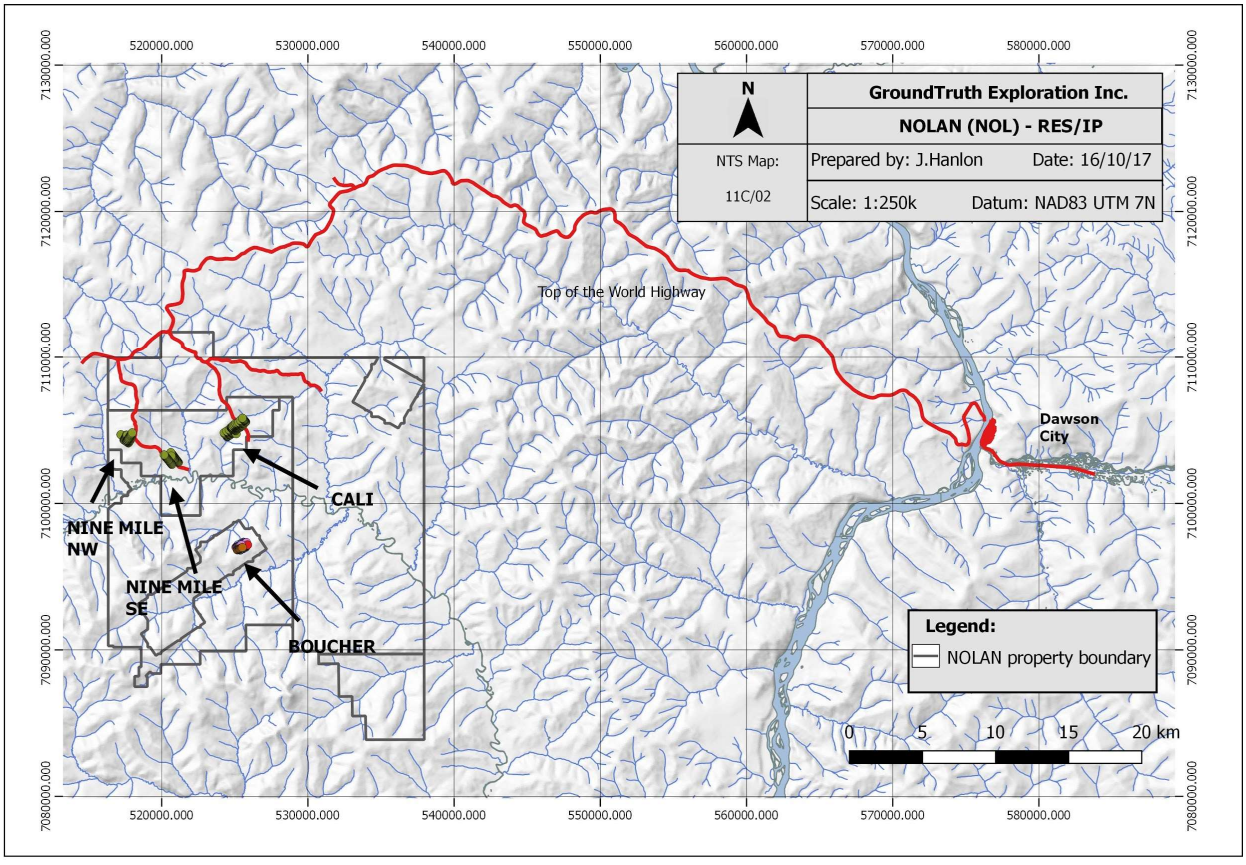

***Figure 1**: Overview map of Nolan 2017 RES/IP grids.*

2.0 Survey Theory

Resistivity and Induced Polarization surveys are an appropriate approach to lode-source gold exploration in Yukon Territories because of the resistivity contrasts inherent to the mineralization and geological structures that are associated with gold deposits. The non-invasive nature of RES/IP combined with its cost efficiency make it a valuable contribution to exploration efforts.

RES/IP surveys involve current injection from the ground surface to induce an electric field that is a function of the conductivity distribution in the subsurface. A current injection typically uses one sink electrode and one source electrode. A measurement of potential field is then acquired across two electrodes that are different from the current electrodes. Hundreds of potential field measurements are made at intervals along the RES/IP traverse for successive current injections to generate the final raw profile of apparent subsurface resistivity.

There are a wide number of array types used to perform RES/IP surveys, each involving a different configuration of current and potential electrodes. Different arrays have strengths and weaknesses in regards to the time necessary to complete the survey and the measurement sensitivity to vertical or horizontal subsurface features. GroundTruth utilizes an extended dipole-dipole array for the NOL project to adequately image the target zones. Details on the extended dipole-dipole array can be found in Appendix C.

2.1 Field Survey Operating Procedure

A crew of 5 GroundTruth personnel sets up and operates each survey. Brief operating procedures are as follows:

1. The midpoint of a traverse is located and the length of the line is sighted using a compass and GPS.
2. Minimal brush is cut along the line to place pickets and set up equipment.
3. 84 electrodes are diligently inserted into the ground, equivalently spaced along the line at 5m and hammered to a depth of 50cm (10% of electrode spacing).
4. Calcium Chloride (CaCl, 25% solution) is added to the base of all electrodes.
5. Cables are laid and connected to the electrodes.
6. Contact resistance test is conducted.
7. Extra electrodes and CaCl solution is added to each electrode with CR >2,000 Ohms. CR test is repeated.
8. Continue to add electrodes and CaCl until satisfactory CR values are achieved.
9. Operator initializes survey.

10. Operator uses DGPS and data collection software to document survey line parameters incl. electrode locations, topography, and notable geological/cultural features if present. Pickets are placed along the line every 50m.
11. Crew cuts and prepares the next survey line.

2.2 Data Processing

Immediately after each survey is completed in the field, the data measurements are downloaded and reviewed for integrity. Any field errors are thus addressed before moving the equipment. RES/IP datasets are processed daily by the lead operator using EarthImager2D software provided by Advanced Geosciences Inc. Outlier/noisy data are removed and the cleaned dataset is inverted. Terrain correction to the inversion mesh is applied from topographic measurements collected in the field using a differential GPS. All raw data from the DGPS and SuperSting are archived for future consultation.

3.0 Survey Personnel and Program Dates

3.1 Survey Personnel

The following table summarizes the GroundTruth personnel involved in completing the survey lines on each of the four Nolan subproperties. Note that on the Nine Mile NW the GroundTruth team was composed of four personnel, instead of the usual five.

Personnel	Position	Cali	Nine Mile SE	Nine Mile NW	Boucher
Jen Hanlon	Lead Geophysical Operator and Crew Chief	✓	✓	✓	✓
Norbert Kapa	Secondary Lead	✓	✓	✓	✓
Pawel Kapa	Geo Technician	✓	✓	✓	✓
Andrew Truax	Geo Technician	✓	✓	✓	✓
Andrew Savage	Geo Technician				✓

Tim Wohlsclagel	Geo Technician	✓	✓		

***Table 1**: Summary of GroundTruth personnel involved in the RES/IP data acquisition on the Nolan subproperties (Cali, Nine Mile SE, Nine Mile NW, and Boucher).*

3.2 Program Dates

Cali:

Mobilize	June 10th
Field Surveys	June 11th - June 19th

Nine Mile SE:

Mobilize	June 20th
Field Surveys	June 21th – June 25th
Demobilize to Dawson	June 26th

Nine Mile NW:

Mobilize	July 9th
Field Surveys	July 10th – July 16th

Boucher:

Mobilize	July 17th
Field Surveys	July 18th – July 21st
Demobilize to Dawson	July 22th

4.0 Cali

4.1 Survey Summary

An overview of the RES/IP grid on the Cali is shown in Figure 2. Brief specifications about the survey lines are outlined below.

Lines:	NOLIP17-01 – NOLIP17-12**
Number of Electrodes	84
Electrode Spacing	5m

Line Length	415m
Array	Extended dipole-dipole

***Note on NOLIP17-04: This line was intended to be a rollalong survey extending 695m, however the data acquired on the rolls are not reliable due to technical difficulties in the field, and so are not included in the report. The length of this line is standard (415m), however the electrode orientation is reversed (i.e. increasing north to south). The electrode orientation of the other lines increases south to north.*

On the NW side of the saddle, the near-surface terrain in the grid area is relatively damp, rocky, and covered by a thin discontinuous layer of permafrost. On the SE side of the saddle, the terrain is drier and quite rocky, particularly near the middle of the survey traverses. This lead to different zones of contact resistance (CR) along each traverse. As expected, the soil-rich areas has lower CR values (generally 1,000–2,500 Ohms), whereas the rockier areas have a higher range of CR values (generally 3,000–6,000 Ohms). In situations where one side of the traverse had better contacts than the other, the array measurement direction was chosen to read from low to high CR.

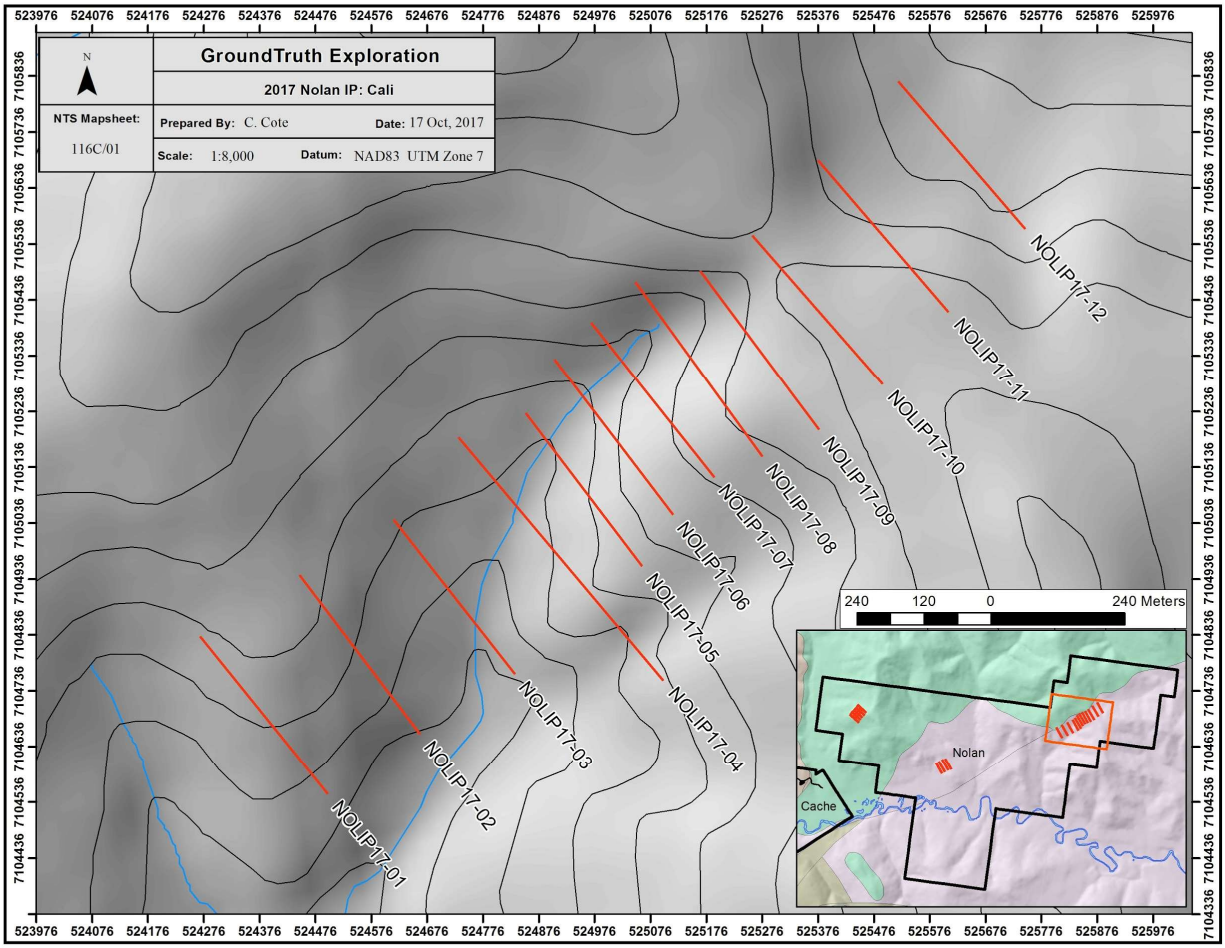

***Figure 2**: 2017 completed RES/IP grid on the Cali zone. Note that NOLIP17-04 is a rollalong survey.*

4.2 Survey Results

The following figures display the inverted resistivity and induced polarization results along each traverse in the Cali zone. Note that the depth of penetration of the IP results is generally less than the resistivity results.

(A)

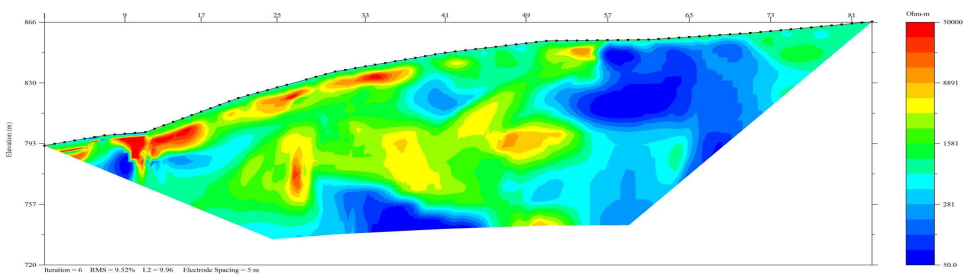

(B)

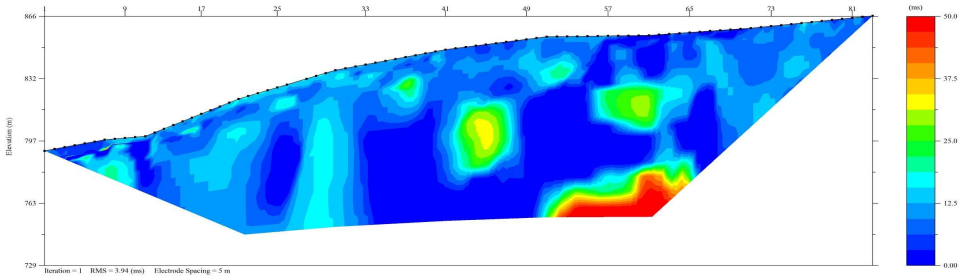

***Figure 3**: NOLIP17-01 sections. (**A**) Inverted resistivity (scale 50-50,000 Ohm-m). (**B**) Inverted IP (scale 0-50 ms).*

(A)

(B)

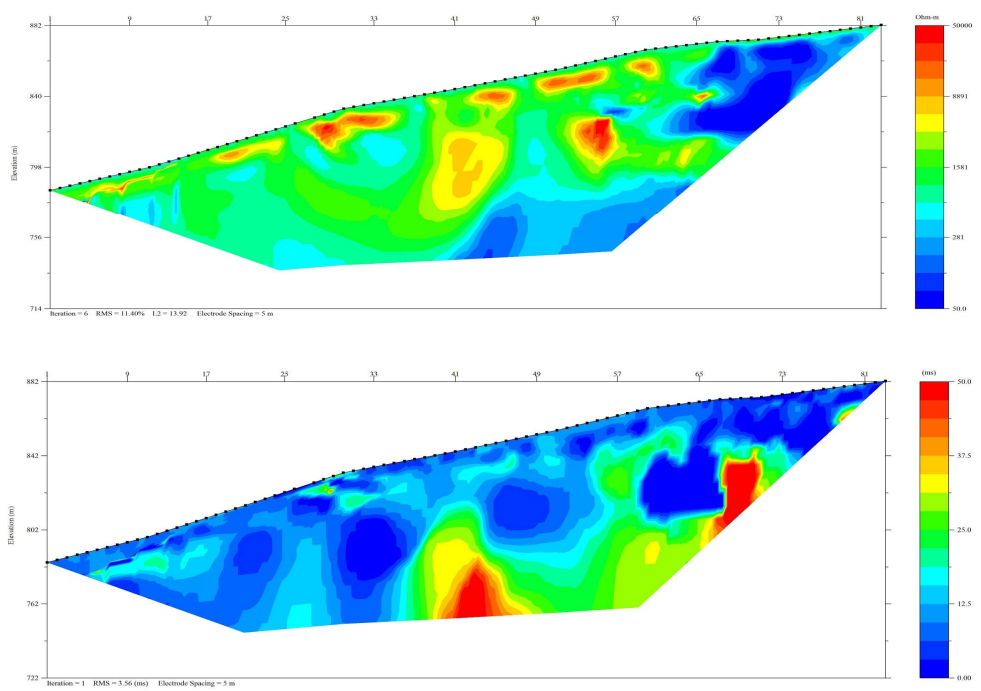

***Figure 4**: NOLIP17-02 sections. (**A**) Inverted resistivity (scale 50-50,000 Ohm-m). (**B**) Inverted IP (scale 0-50 ms).*

(A)

(B)

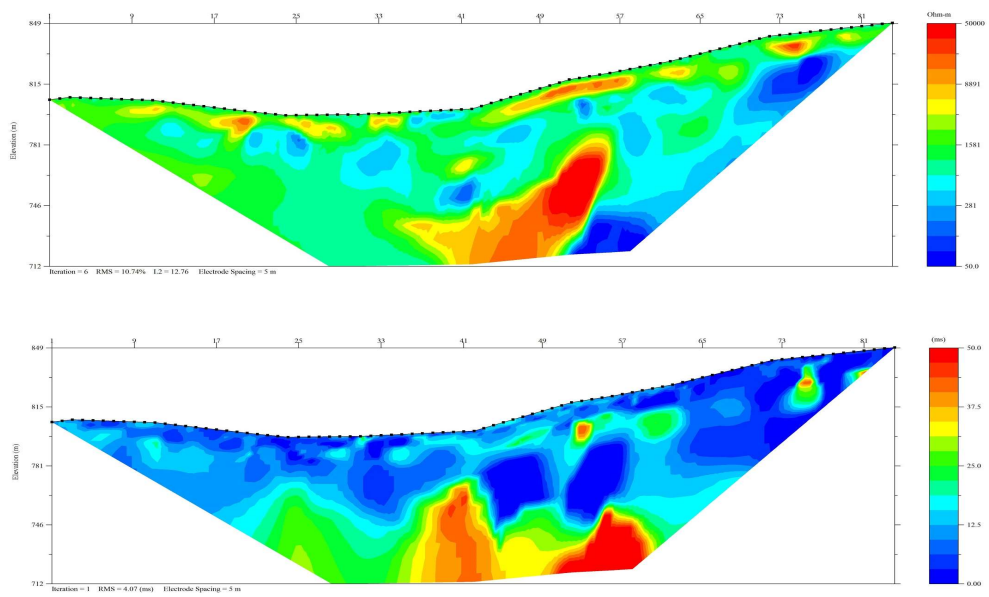

***Figure 5**: NOLIP17-03 sections. (**A**) Inverted resistivity (scale 50-50,000 Ohm-m). (**B**) Inverted IP (scale 0-50 ms).*

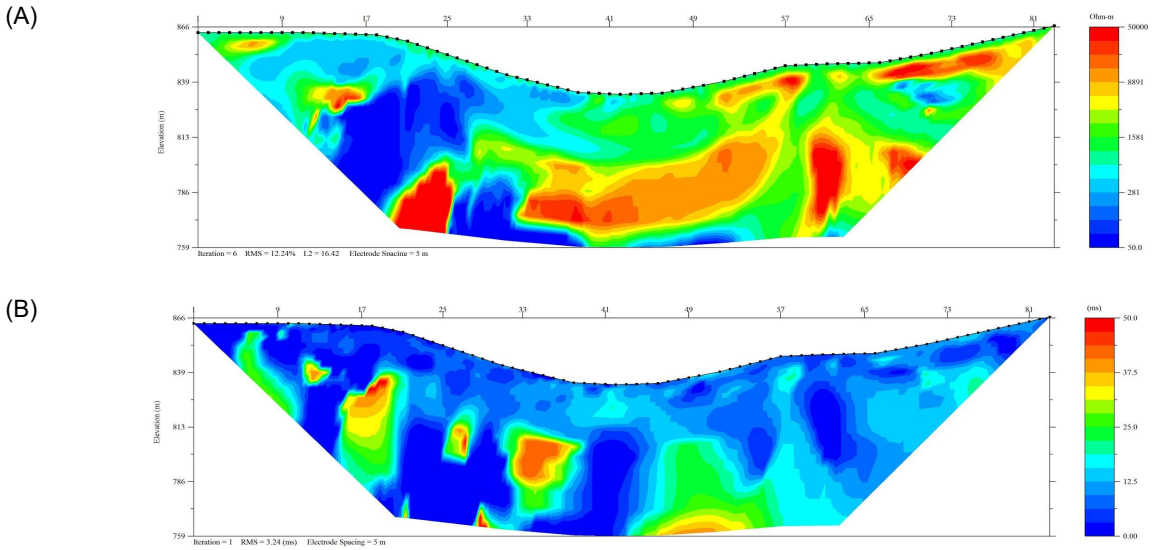

***Figure 6**: NOLIP17-04 sections. (**A**) Inverted resistivity (scale 50-50,000 Ohm-m). (**B**) Inverted IP (scale 0-50 ms). Note that the orientation of this section is opposite to the remainder of the RES/IP sections on the Cali.*

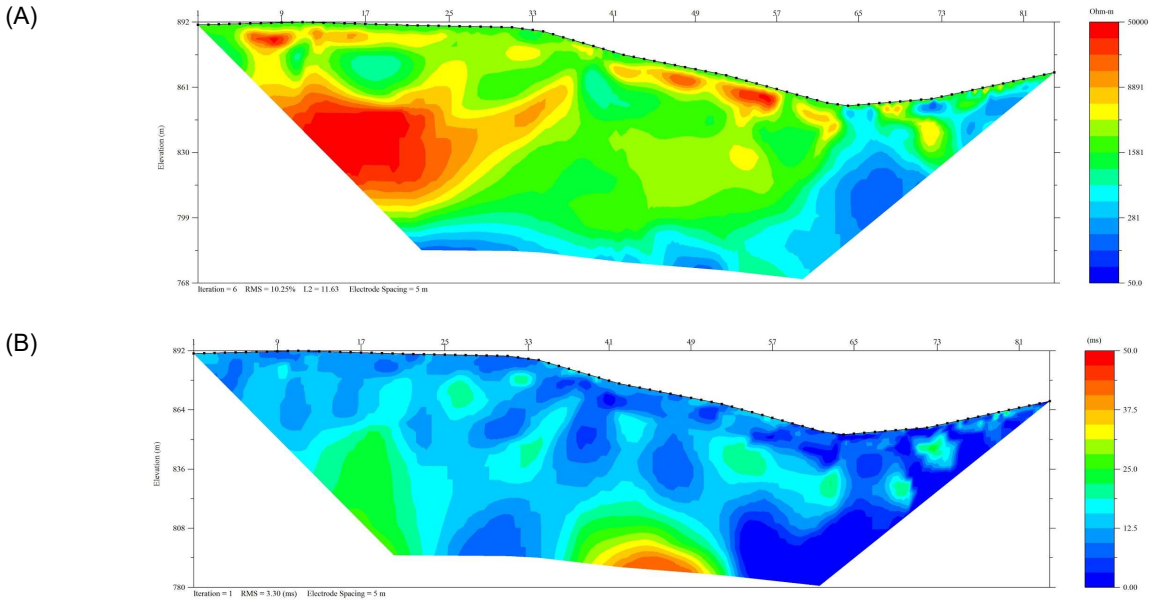

***Figure 7**: NOLIP17-05 sections. (**A**) Inverted resistivity (scale 50-50,000 Ohm-m). (**B**) Inverted IP (scale 0-50 ms).*

(A)

(B)

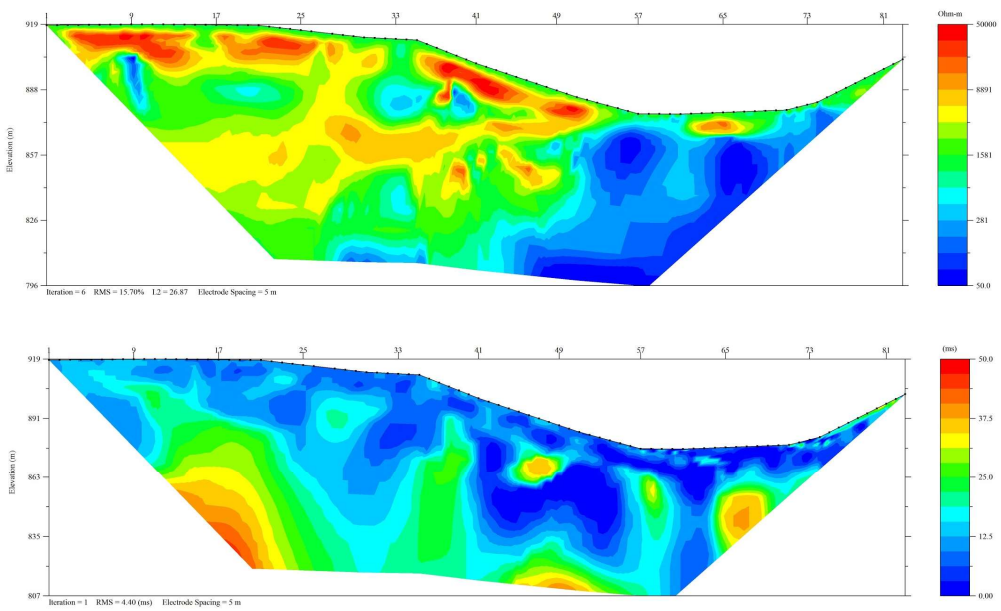

***Figure 8**: NOLIP17-06 sections. (**A**) Inverted resistivity (scale 50-50,000 Ohm-m). (**B**) Inverted IP (scale 0-50 ms).*

(A)

(B)

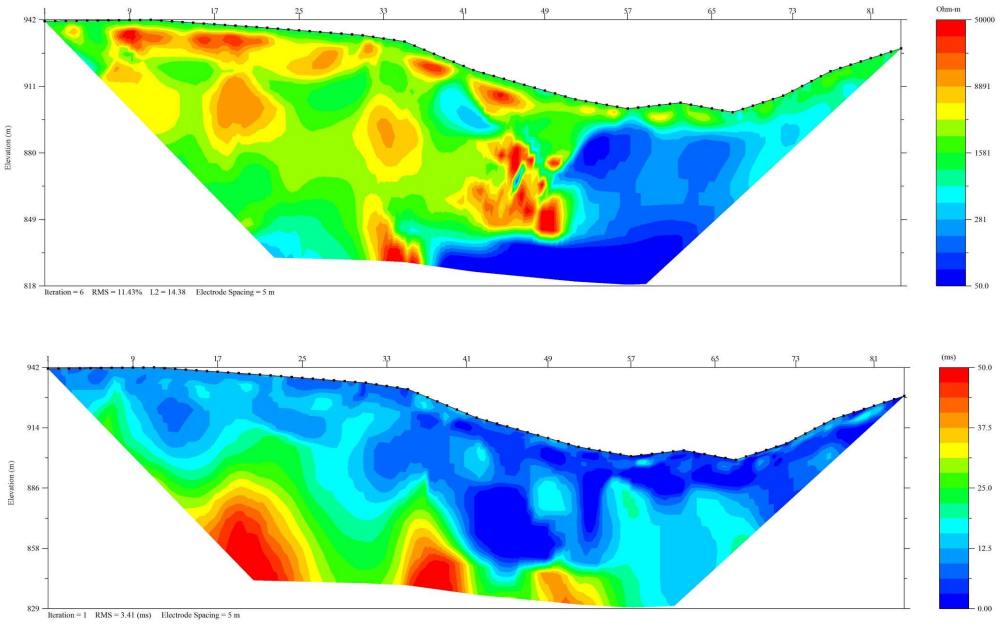

***Figure 9**: NOLIP17-07 sections. (**A**) Inverted resistivity (scale 50-50,000 Ohm-m). (**B**) Inverted IP (scale 0-50 ms).*

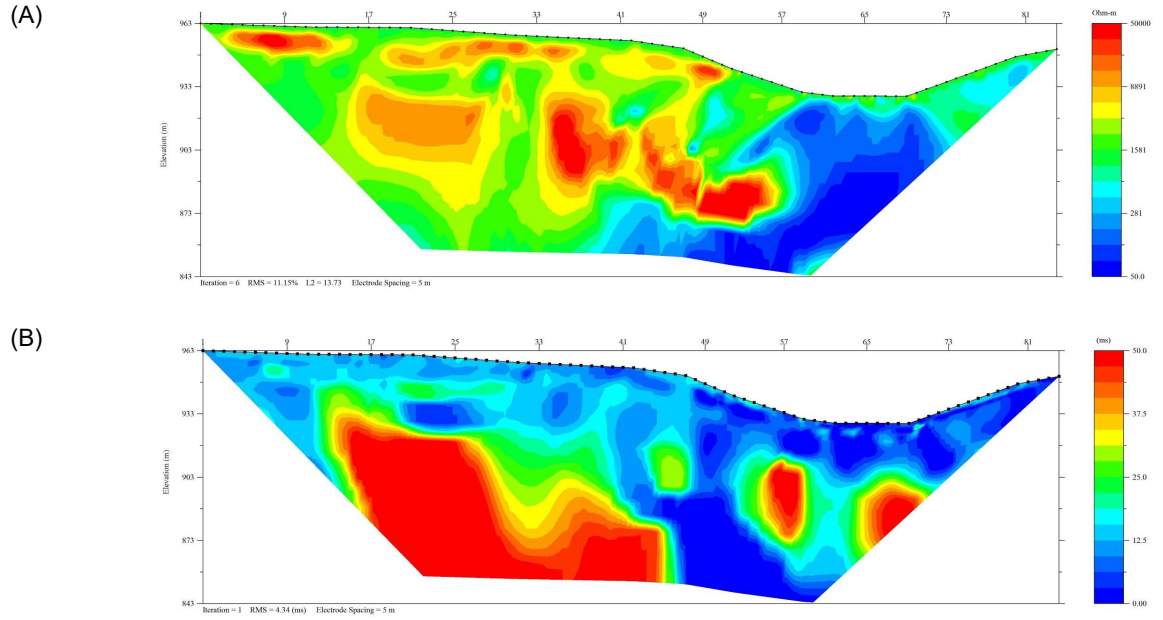

***Figure 10**: NOLIP17-08 sections. (**A**) Inverted resistivity (scale 50-50,000 Ohm-m). (**B**) Inverted IP (scale 0-50 ms).*

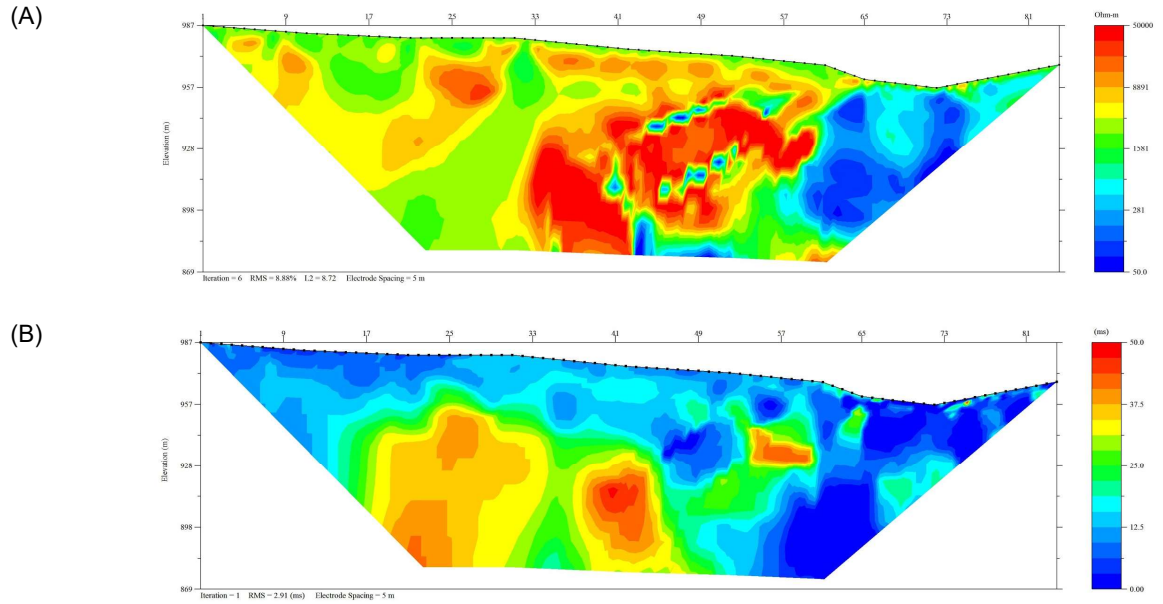

***Figure 11**: NOLIP17-09 sections. (**A**) Inverted resistivity (scale 50-50,000 Ohm-m). (**B**) Inverted IP (scale 0-50 ms).*

(A)

(B)

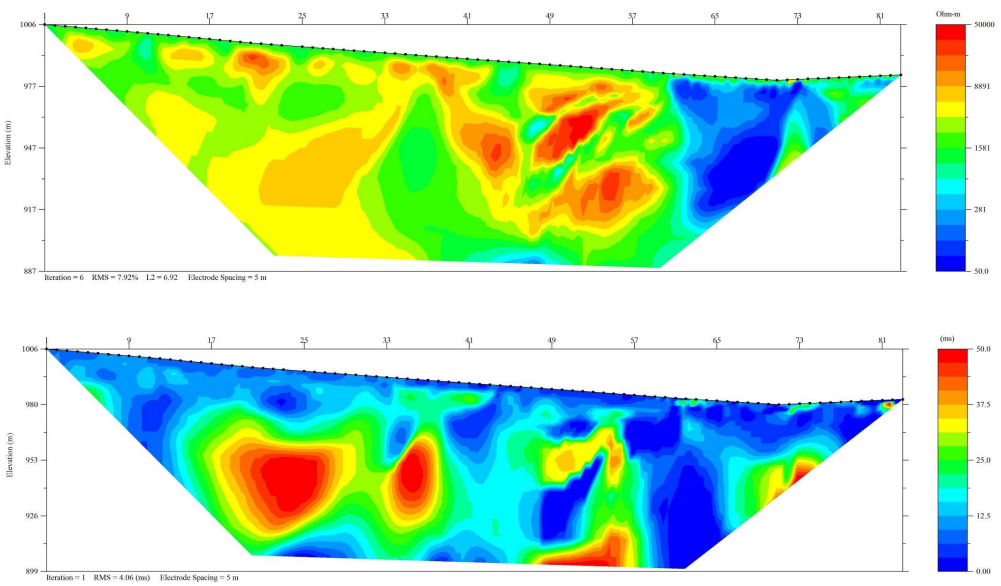

***Figure 12**: NOLIP17-10 sections. (**A**) Inverted resistivity (scale 50-50,000 Ohm-m). (**B**) Inverted IP (scale 0-50 ms).*

(A)

(B)

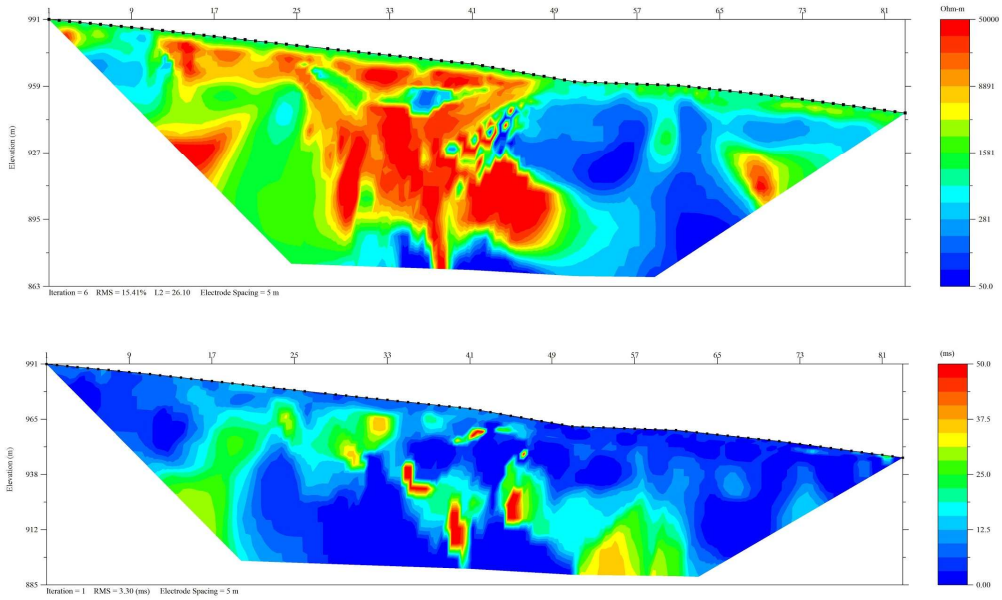

***Figure 13**: NOLIP17-11 sections. (**A**) Inverted resistivity (scale 50-50,000 Ohm-m). (**B**) Inverted IP (scale 0-50 ms).*

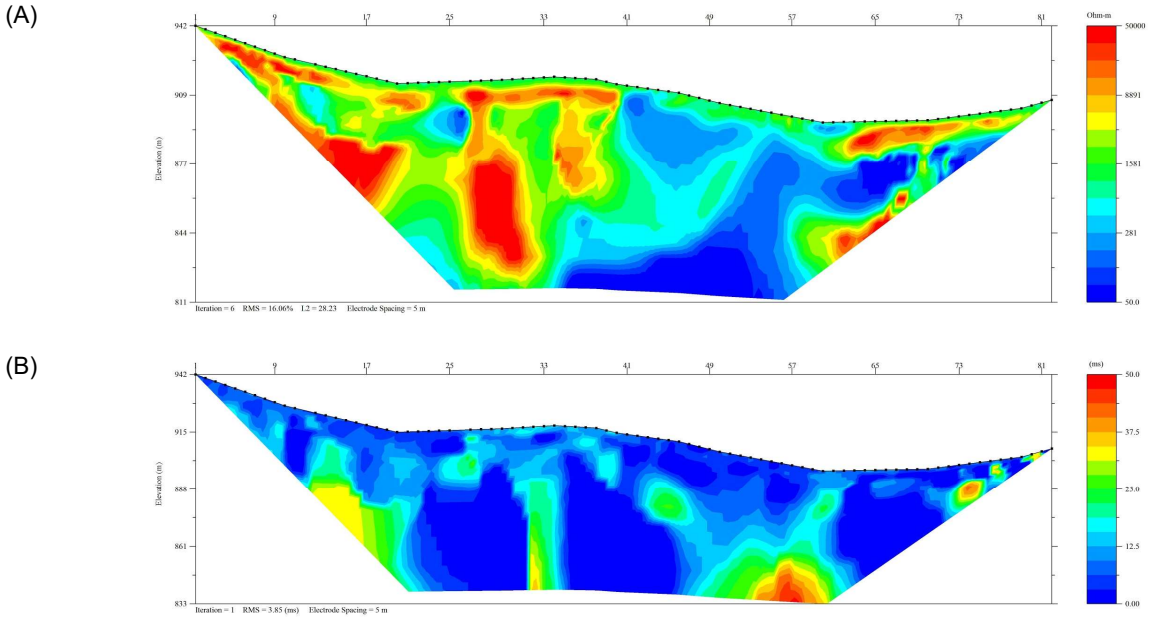

***Figure 14**: NOLIP17-12 sections. (**A**) Inverted resistivity (scale 50-50,000 Ohm-m). (**B**) Inverted IP (scale 0-50 ms).*

4.3 Interpretation

Interpretation of 2-D resistivity and induced polarization surveys first requires identifying anomalous zones that are caused by real subsurface electrical boundaries versus those that are artefacts (formed during the inversion process). Real anomalous zones will trend between adjacent RES/IP lines and show correlation with crossline data. This section provides a brief qualitative description of the electrical conductivity and chargeability anomalies that trend between the RES/IP sections presented in section 4.2.

The resistivity sections show quite clearly a resistive unit on NW side of the grid and a conductive unit on the SE side. The boundary between these units remains distinct at all depths of the sections and appears to trend towards the NW from surface. The high chargeability zones are sporadic throughout the sections, however tend to be located at depth and spread throughout the resistive unit. Sometimes the zones of chargeability highs are also located in the conductive unit and close to the unit boundary.

Similarities between the conductive and resistive units throughout the Cali RES/IP survey lines inflicts confidence that these anomalies define a real subsurface electrical boundary. To further constrain this interpretation, it is recommended that known

geological and geochemical information is incorporated. This will aid the interpreter to gain a better understanding of these anomalies and potentially aid them to find the geological structures and mineralized zones inherent to gold deposits.

5.0 Nine Mile SE

5.1 Survey Summary

An overview of the RES/IP grid on the Nine Mile SE zone is shown in Figure 15. Brief specifications about the survey lines are outlined below.

Lines	NOLIP17-13 – NOLIP17-15
Number of Electrodes	84
Electrode Spacing	5m
Line Length	415m
Array	Extended dipole-dipole

Line	NOLIP17-16
Number of Electrodes	196
Electrode Spacing	5m
Line Length	830m
Array	Extended dipole-dipole

Line	NOLIP17-17
Number of Electrodes	183
Electrode Spacing	5m
Line Length	830m
Array	Extended dipole-dipole

The exact placement of the survey lines on the Nine Mile SE grid maximize coverage of gold-in-soil anomalies and geological structures while not crossing the road that passes through the grid (figure 15). The majority of the grid is covered by slightly rocky and dry terrain. A portion of lines NOLIP17-15 and NOLIP17-16 pass through different bulldozed zones that have a significant portion of cobble-sized rocks at the surface (see figure 3).

Throughout the Nine Mile SE grid electrode contact resistance values are moderate, ranging from approximately 1,000–3,500 Ohms and occasionally up to 4,500 Ohms. In particularly difficult spots the CR extends to >10,000 Ohms, however this occurrence is rare. In situations where one side of the traverse had better contacts than the other, the array measurement direction was chosen to read from low to high CR.

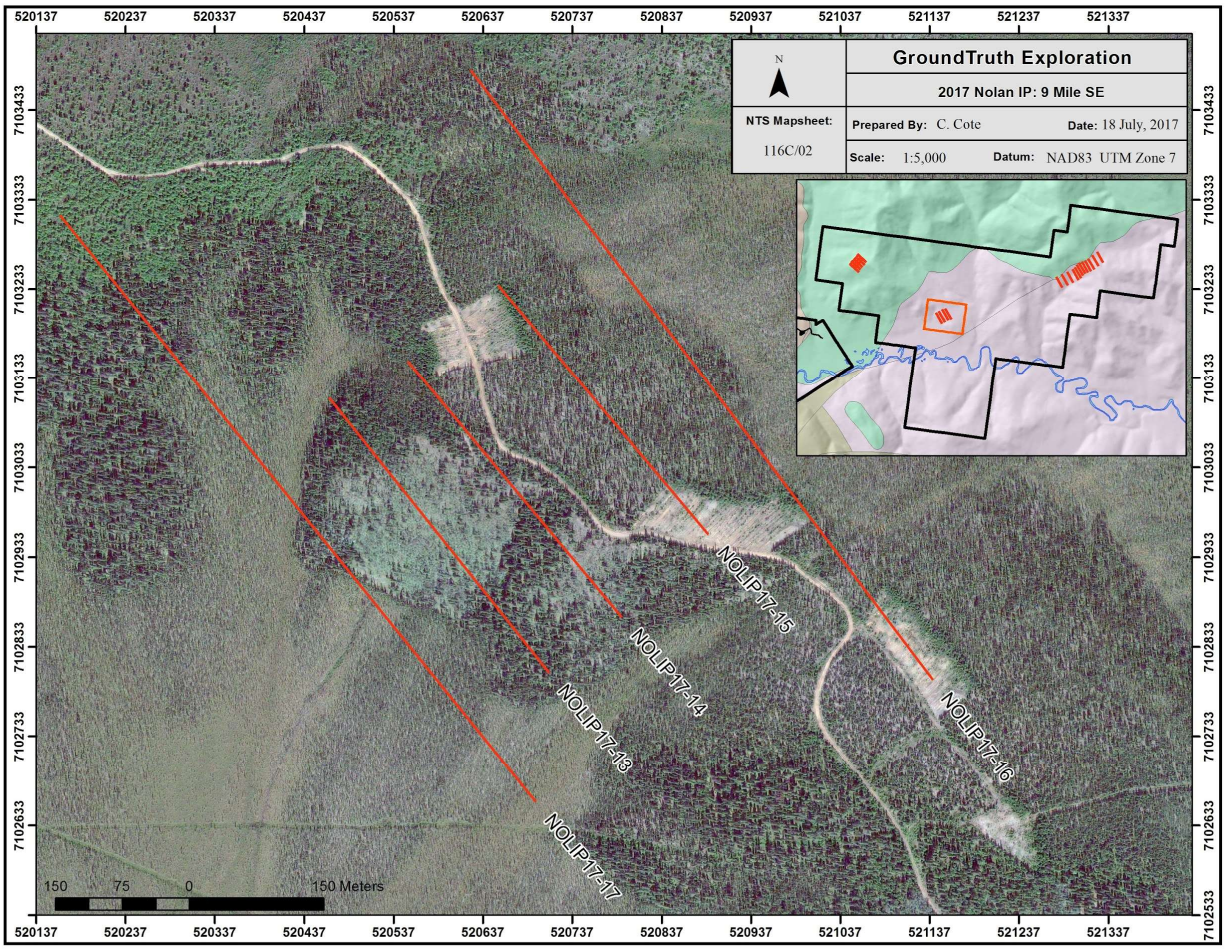

Figure 15: 2017 completed RES/IP grid on the Nine Mile SE. Note that NOLIP17-16 and NOLIP17-17 are rollalong surveys.

5.2 Survey Results

The following figures display the inverted resistivity and induced polarization sections along each traverse in the Nine Mile SE zone. Note that the depth of penetration of the IP results is generally less than the resistivity results.

(A)

(B)

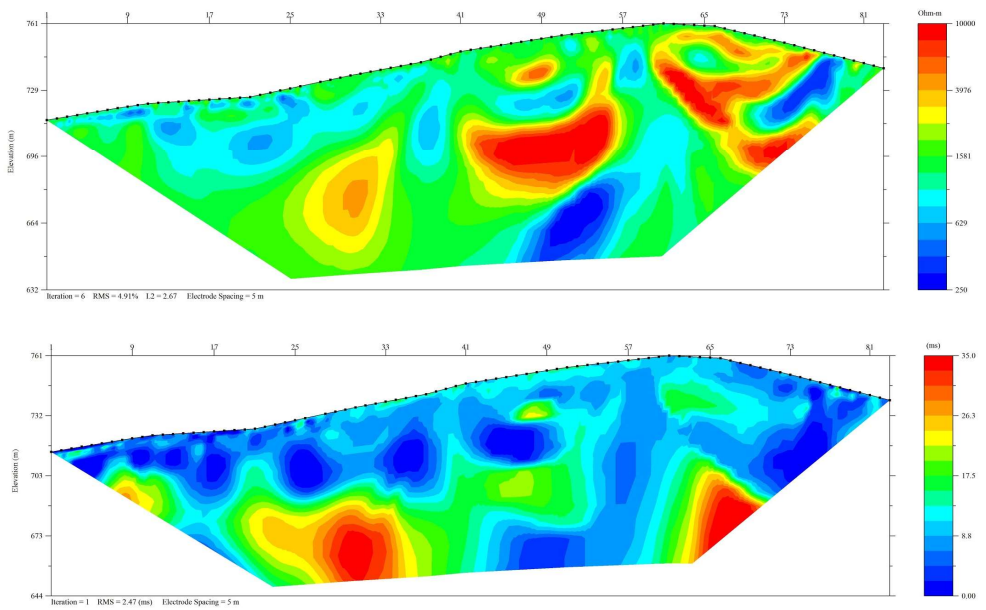

***Figure 16**: NOLIP17-13 sections. (**A**) Inverted resistivity (scale 250-10,000 Ohm-m). (**B**) Inverted IP (scale 0-35 ms).*

(A)

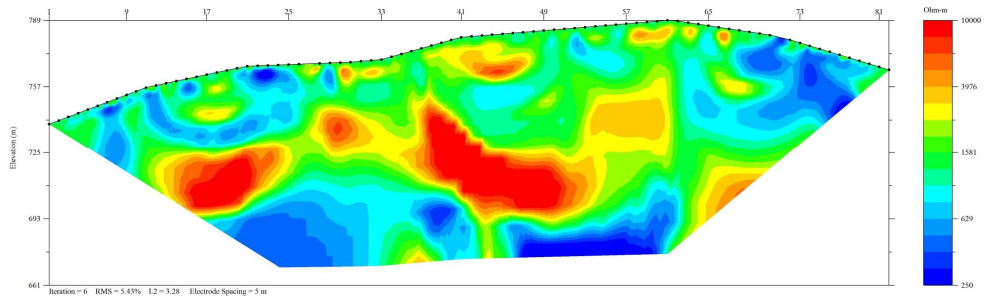

(B)

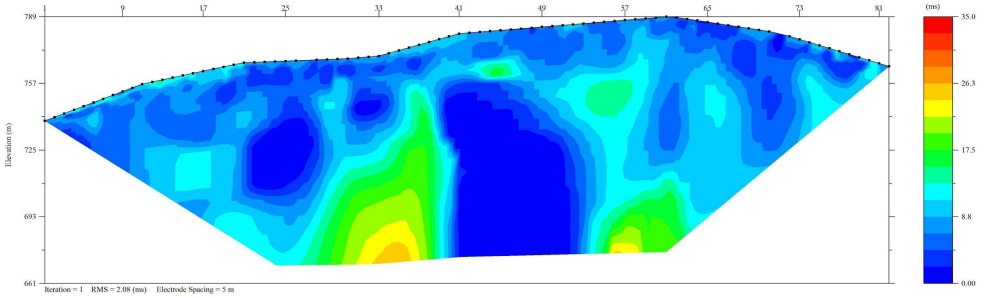

***Figure 17**: NOLIP17-14 sections. (**A**) Inverted resistivity (scale 250-10,000 Ohm-m). (**B**) Inverted IP (scale 0-35 ms).*

(A)

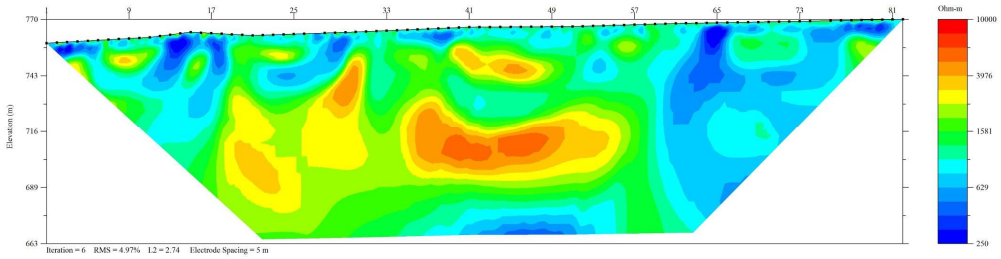

(B)

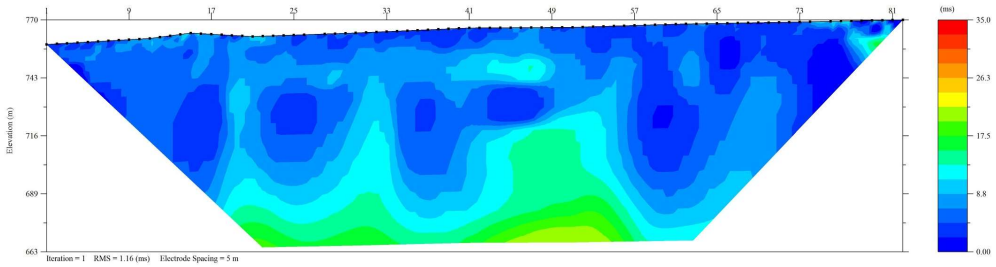

***Figure 18**: NOLIP17-15 sections. (**A**) Inverted resistivity (scale 250-10,000 Ohm-m). (**B**) Inverted IP (scale 0-35 ms).*

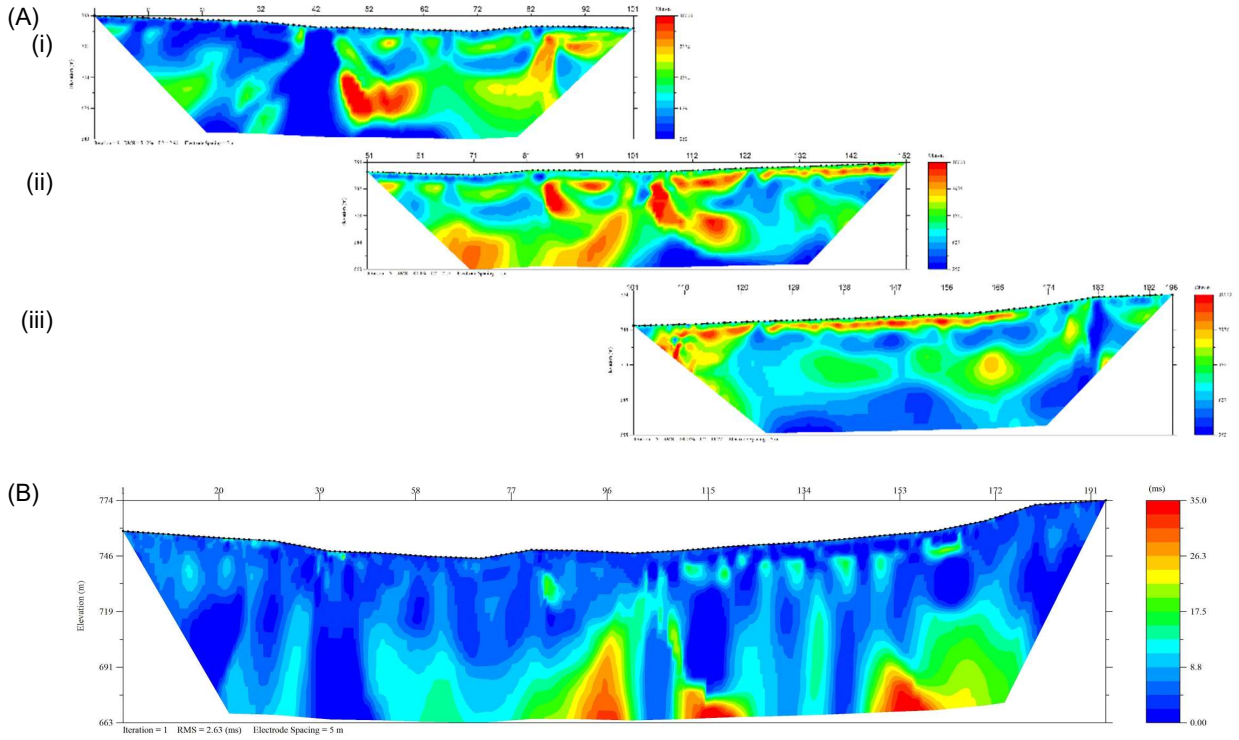

***Figure 19**: NOLIP17-16 rollalong sections. (**A**) Inverted resistivity (scale 250-10,000 Ohm-m). Due to processing limitations this section had to be split into three subsets of data: (i) electrodes 1-101, (ii) electrodes 51-152, and (iii) electrodes 101-196. (**B**) Inverted IP (scale 0-35 ms).*

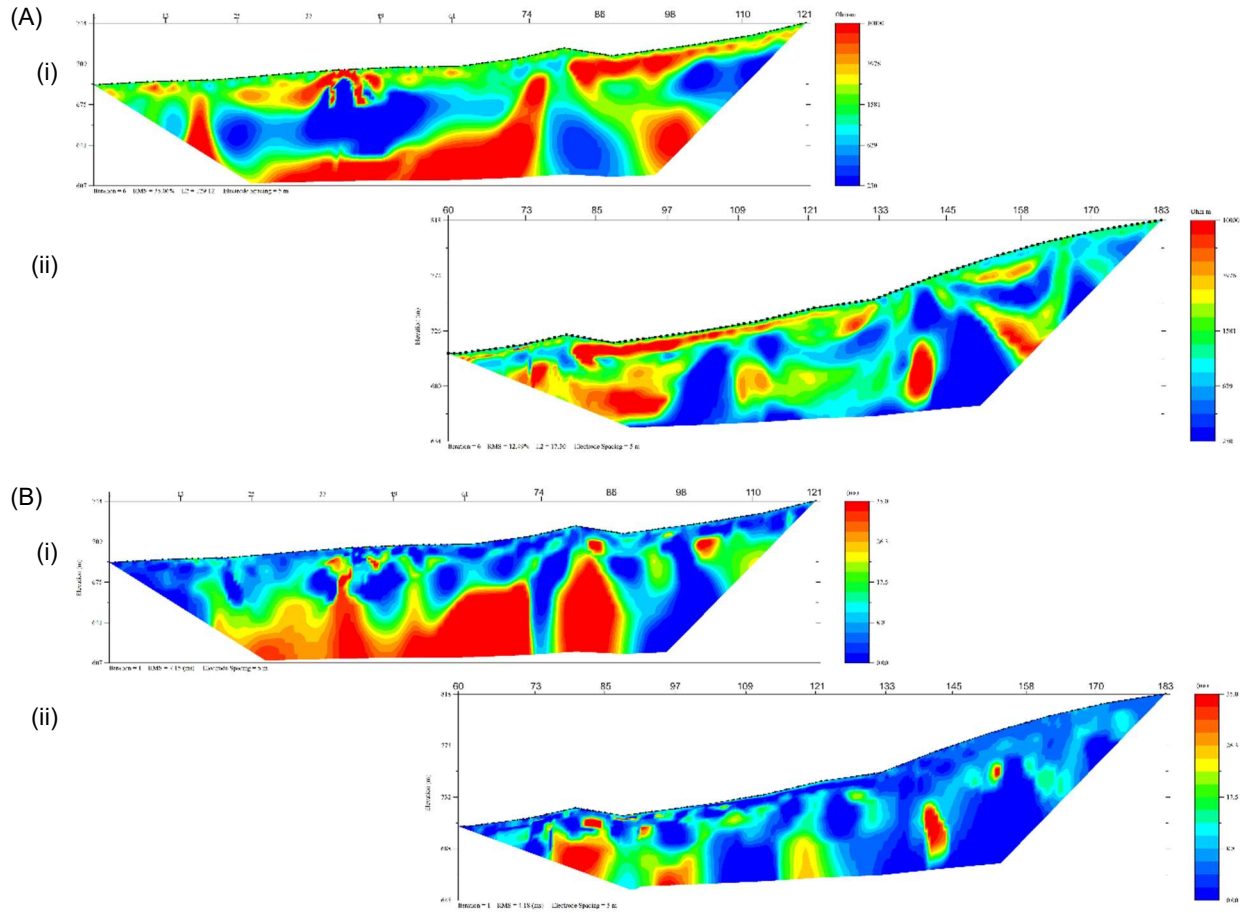

***Figure 20**: NOLIP17-17 rollalong sections. (**A**) Inverted resistivity (scale 250-10,000 Ohm-m). (**B**) Inverted IP (scale 0-35 ms). Due to processing limitations, each (A) and (B) had to be split into two subsets of data for inversion: (i) electrodes 1-121, and (ii) electrodes 60-183.*

5.3 Interpretation

Qualitatively, the 2-D RES/IP surveys acquired in the Nine Mile SE zone show similar zones of resistivity and chargeability between the profiles. Each of the 415m surveys seem to be located over sporadic resistive lenses that form an overall relatively resistive zone. The rollalong survey NOLIP17-16 indicates that this resistive zone is sandwiched in between more conductive zones to the north and south. The rollalong survey NOLIP17-17 is located further north than the others, and shows definite conductive and resistive lenses to the south and the subsurface becomes more conductive to the north. To further constrain this interpretation, it is recommended that known geological and

geochemical information is incorporated about the site. This will aid the interpreter to gain a better understanding of these anomalies and potentially aid them to identify geological structures and mineralized zones inherent to gold deposits.

6.0 Nine Mile NW

6.1 Survey Summary

An overview of the 2017 RES/IP grid on the Nine Mile NW zone is shown in Figure 21. Brief specifications about the survey lines are outlined below.

Lines	NOLIP17-18, -19, -21, -22, -24
Number of Electrodes	84
Electrode Spacing	5m
Line Length	415m
Array	Extended dipole-dipole

Line	NOLIP17-20
Number of Electrodes	168
Electrode Spacing	5m
Line Length	750m
Array	Extended dipole-dipole

Line	NOLIP17-23
Number of Electrodes	154
Electrode Spacing	5m
Line Length	725m
Array	Extended dipole-dipole

Placement of the survey lines on the Nine Mile NW grid maximize coverage of gold-in-soil anomalies and geological structures. Two crosslines (NOLIP17-23 and NOLIP17-24) are utilized to gain sufficient spatial insight to the distribution of subsurface structures.

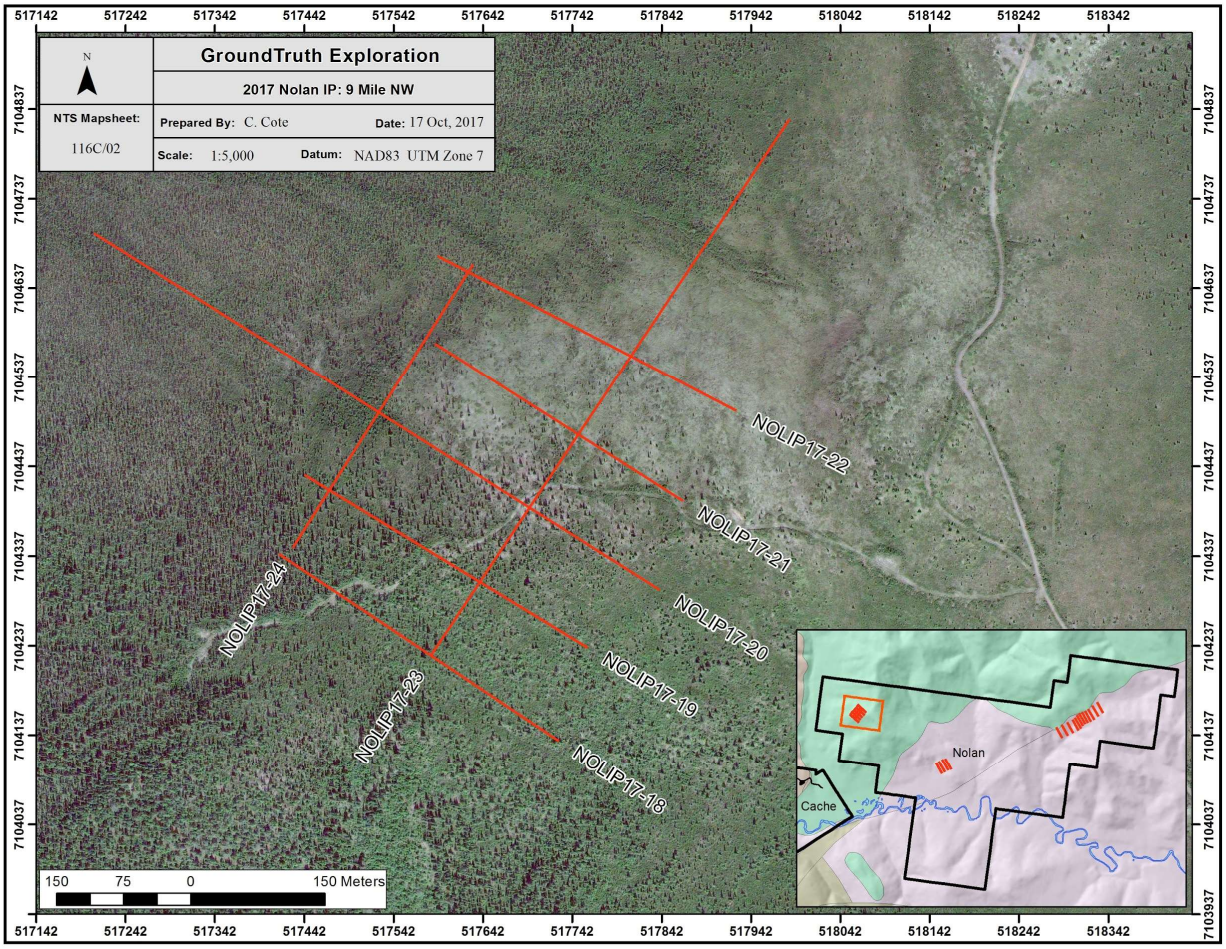

***Figure 21**: 2017 completed RES/IP grid on the Nine Mile NW zone. Note that NOLIP17-20 and NOLIP17-23 are rollalong surveys.*

The majority of the grid near-surface is covered by rocky and dry, unconsolidated soil. Despite careful electrode placement and saturation with calcium chloride solution, these ground conditions lead to relatively high electrode contact resistance values throughout the grid. Most values ranged between 3,000–7,000 Ohms and particularly boulder-rich ground reached values upwards of 10,000 Ohms. Along a few traverses the electrode contacts were not sufficient to collect worthwhile IP data and thus that information is not presented in this report. In situations where one side of the traverse had better contacts than the other, the array measurement direction was chosen to read from low to high CR.

6.2 Survey Results

The following figures display the inverted resistivity and induced polarization sections along each traverse in the Nine Mile NW zone. Note that the depth of penetration of the IP results can be notably less than the resistivity results.

(A)

(B)

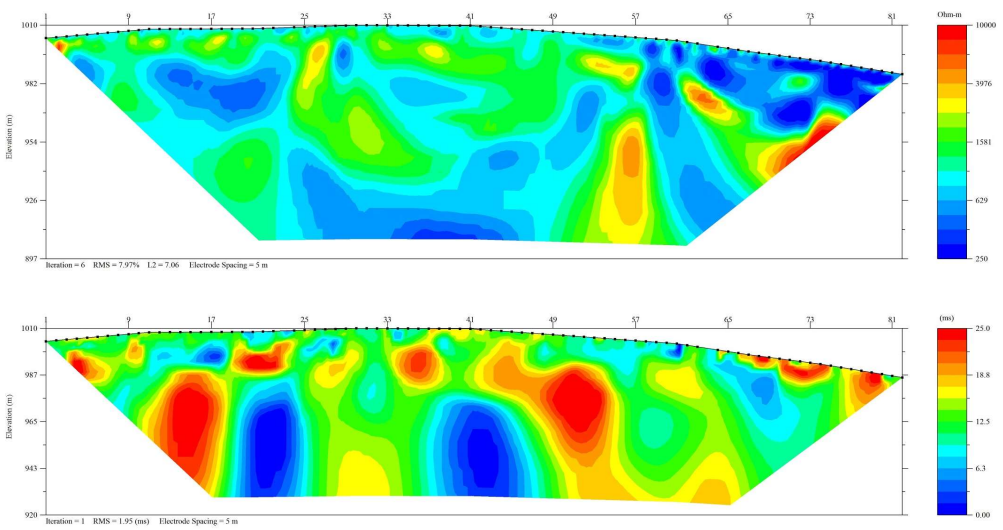

***Figure 22**: NOLIP17-18 sections. (**A**) Inverted resistivity (scale 250-10,000 Ohm-m). (**B**) Inverted IP (scale 0-25 ms).*

(A)

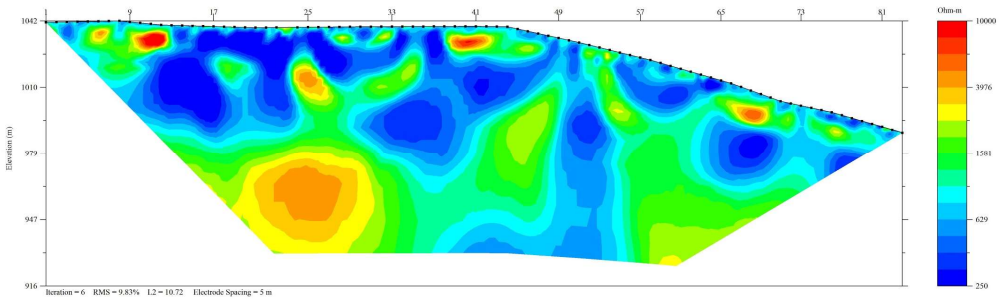

***Figure 23**: NOLIP17-19 section. (**A**) Inverted resistivity (scale 250-10,000 Ohm-m).*

(A)

(B)

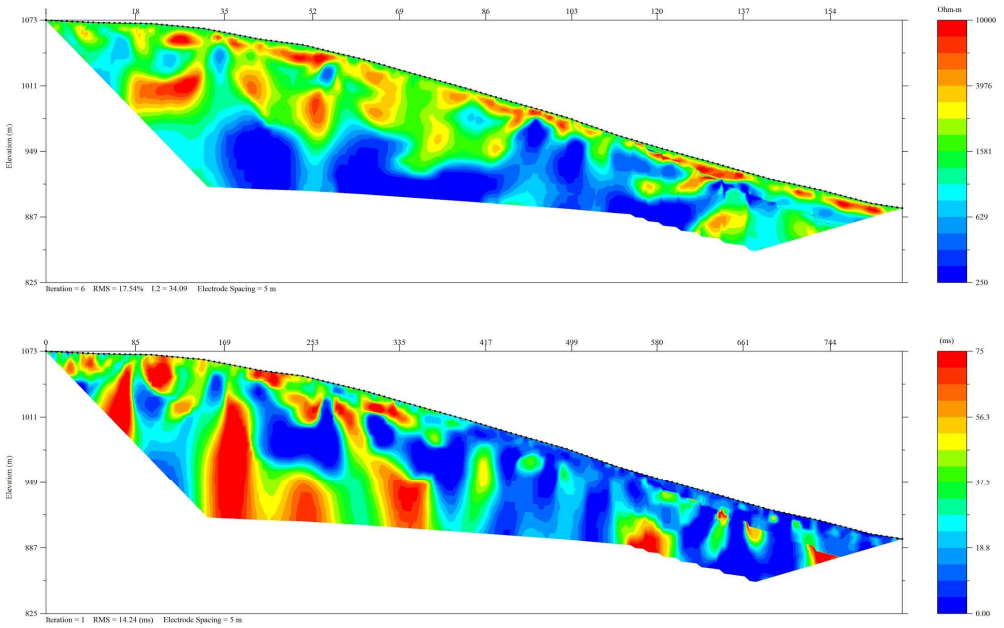

***Figure 24**: NOLIP17-20 rollalong sections. (**A**) Inverted resistivity (scale 250-10,000 Ohm-m). (**B**) Inverted IP (scale 0-75 ms).*

(A)

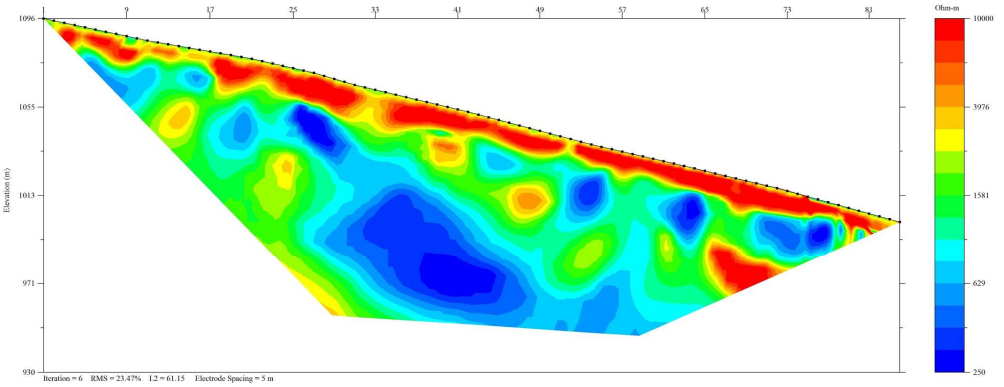

***Figure 25**: NOLIP17-21 sections. (**A**) Inverted resistivity (scale 250-10,000 Ohm-m).*

(A)

(B)

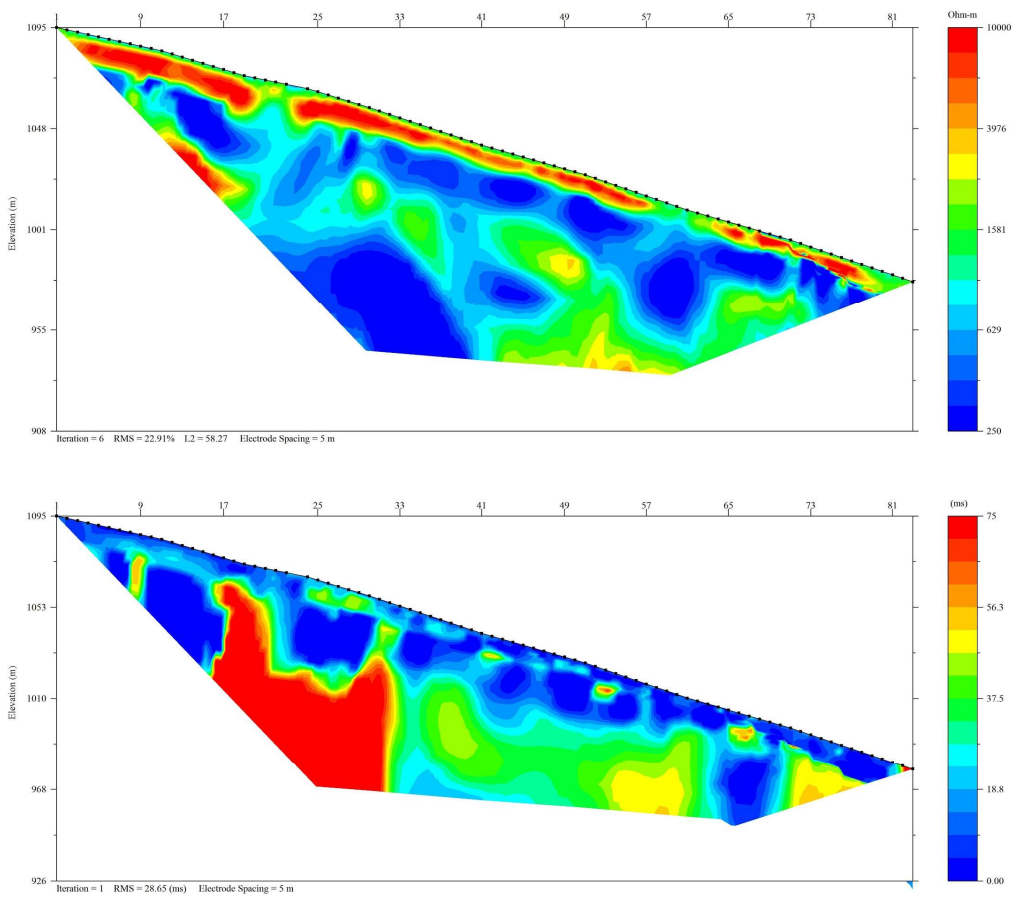

***Figure 26**: NOLIP17-22 sections. (**A**) Inverted resistivity (scale 250-10,000 Ohm-m). (**B**) Inverted IP (scale 0-75 ms).*

(A)

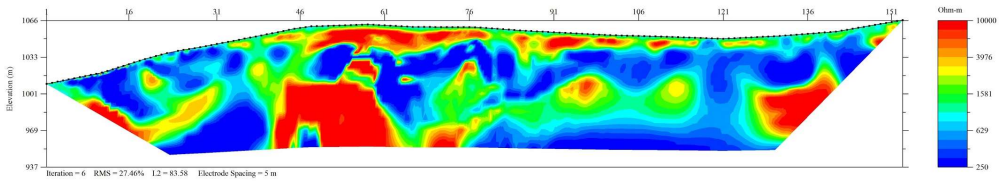

***Figure 27**: NOLIP17-23 rollalong section. (**A**) Inverted resistivity (scale 250-10,000 Ohm-m).*

(A)

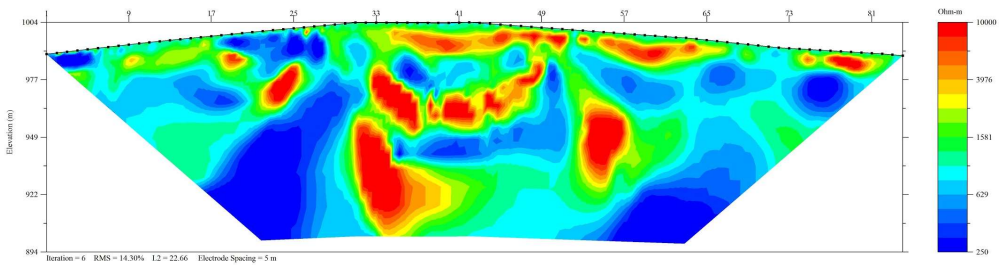

***Figure 28**: NOLIP17-24 section. (**A**) Inverted resistivity (scale 250-10,000 Ohm-m).*

6.3 Interpretation

Qualitatively, the 2-D RES/IP surveys acquired in the Nine Mile NW zone show decent correlation between subsurface resistivity anomalies. Correlation between chargeability anomalies is harder to interpret because reliable IP data was not able to be obtained on four of the seven traverses.

In general there is progression towards a more resistive upper ground surface layer towards the northeast side of the grid. Deeper ground material have conductive zones that dip towards the southeast mixed with more resistive zones. To further constrain this interpretation, it is recommended that known geological and geochemical information is incorporated about the site. This will aid the interpreter to gain a better understanding of these anomalies and potentially aid them to identify geological structures and mineralized zones inherent to gold deposits.

7.0 Boucher

7.1 Survey Summary

An overview of the 2017 RES/IP grid on the Boucher zone is shown in Figure 29. Brief specifications about the survey lines are outlined below.

Lines	BOUIP17-25, -27, -28, -30, -32, -33, -34
Number of Electrodes	84
Electrode Spacing	5m
Line Length	415m
Array	Extended dipole-dipole

Placement of the survey lines on the Boucher grid maximize coverage of gold-in-soil anomalies and geological structures. Three crosslines (BOUIP17-32, BOUIP17-33, and BOUIP17-34) are utilized to gain sufficient spatial insight to the distribution of subsurface structures.

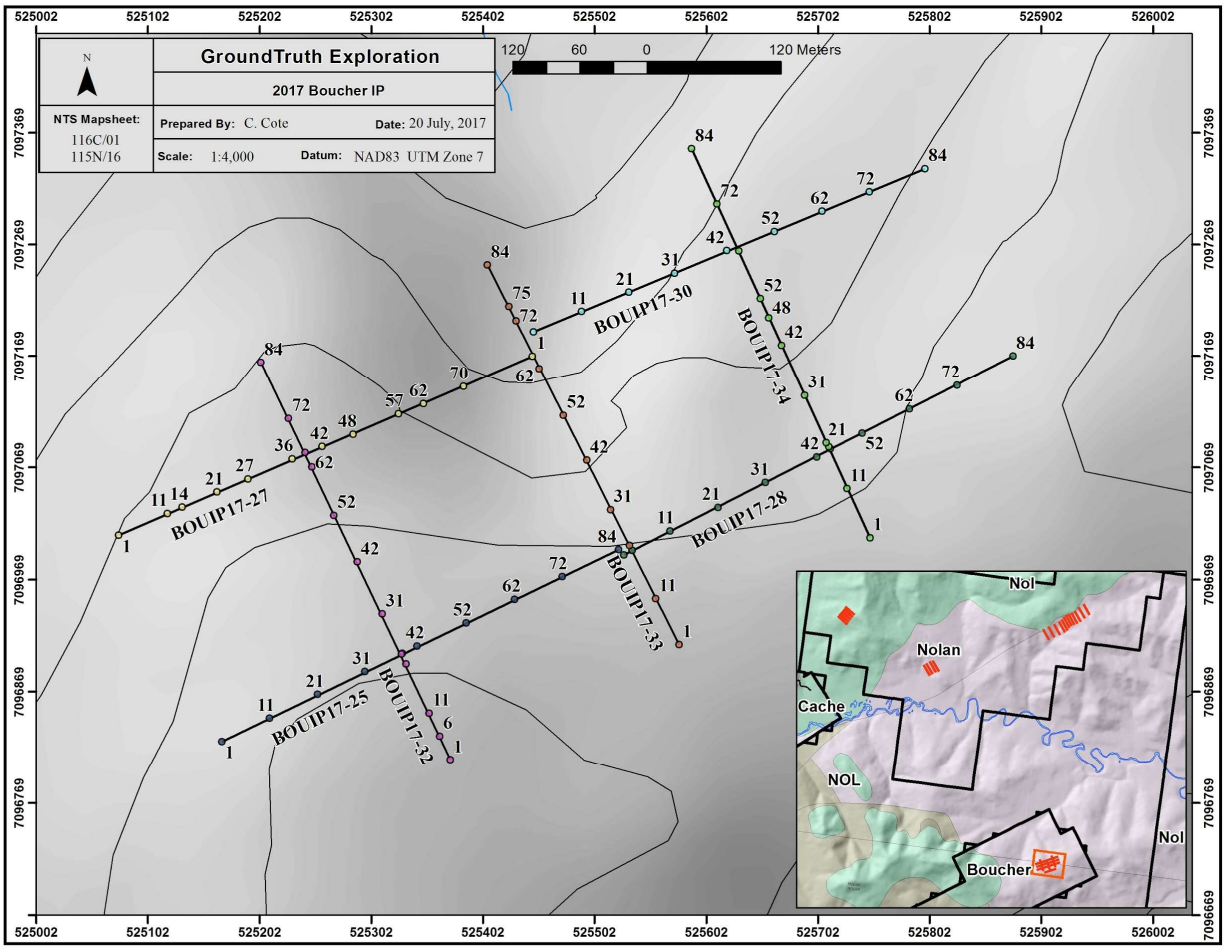

***Figure 29**: 2017 completed RES/IP grid on the Boucher subproperty of the Nolan.*

The majority of the grid near-surface is covered by a variety of grass and moss-covered damp to dry unconsolidated soil. Each electrode was carefully placed and saturated with calcium chloride solution to achieve the lowest possible contact resistance values throughout the grid. Most values ranged between 1,500–7,500 Ohms, and some values reached upwards of 9,500 Ohms in areas with high root density (in which it is difficult to achieve consistent contact along the entire electrode length). In situations where one

side of the traverse had better contacts than the other, the array measurement direction was chosen to read from low to high CR.

7.2 Survey Results

The following figures display the inverted resistivity and induced polarization sections along each traverse in the Boucher zone. Note that the depth of penetration of the IP results can be notably less than the resistivity results.

(A)

(B)

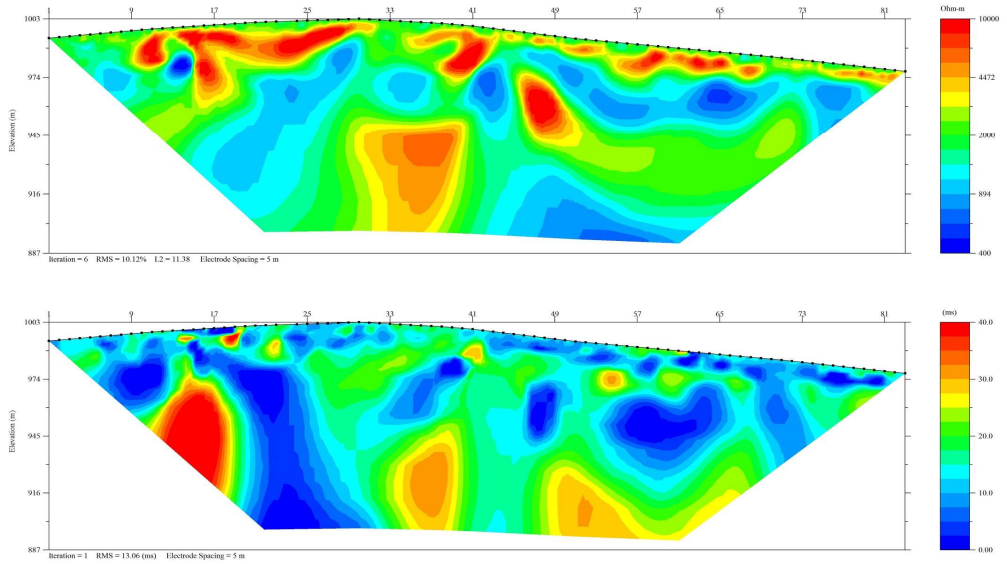

***Figure 30**: NOLIP17-25 sections. (**A**) Inverted resistivity (scale 400-10,000 Ohm-m). (**B**) Inverted IP (scale 0-40 ms).*

(A)

(B)

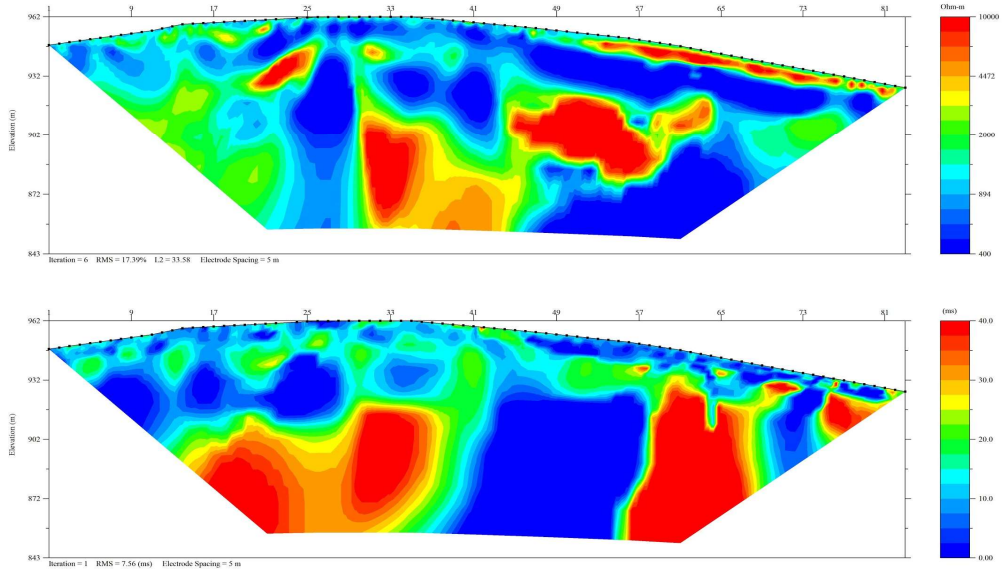

***Figure 31**: NOLIP17-27 sections. (**A**) Inverted resistivity (scale 400-10,000 Ohm-m). (**B**) Inverted IP (scale 0-40ms).*

(A)

(B)

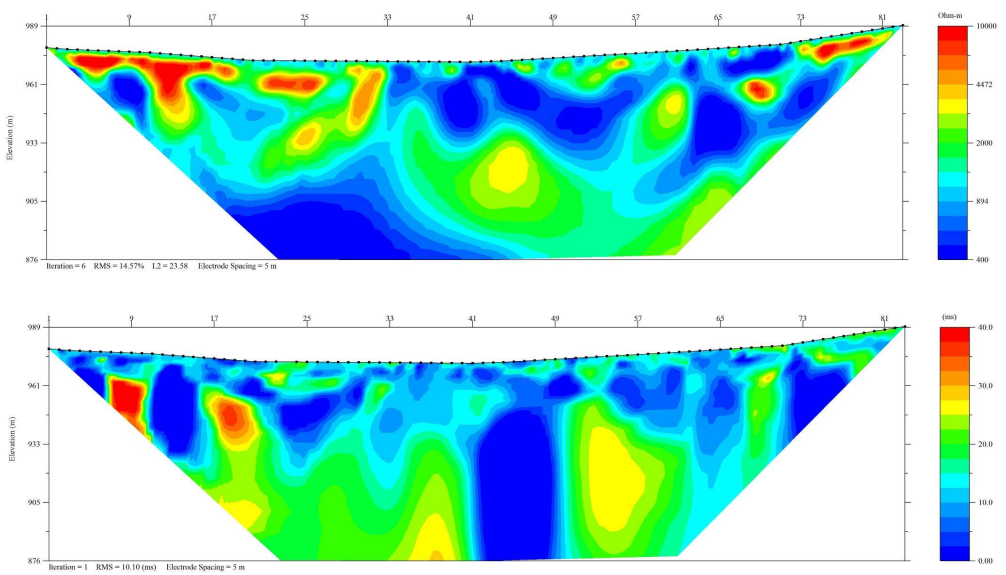

***Figure 32**: NOLIP17-28 sections. (**A**) Inverted resistivity (scale 400-10,000 Ohm-m). (**B**) Inverted IP (scale 0-40 ms).*

(A)

(B)

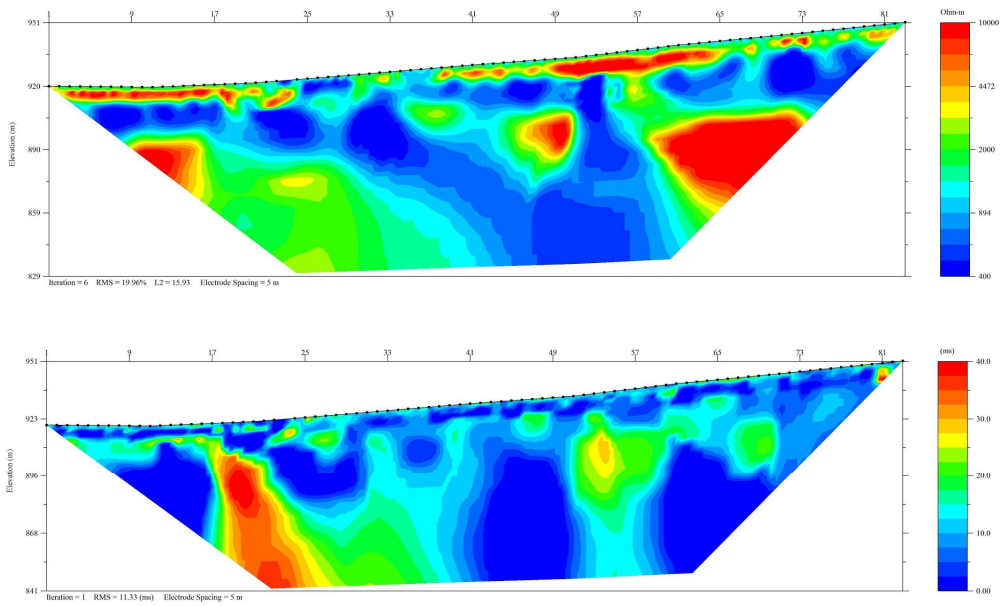

***Figure 33**: NOLIP17-30 sections. (**A**) Inverted resistivity (scale 400-10,000 Ohm-m). (**B**) Inverted IP (scale 0-40 ms).*

(A)

(B)

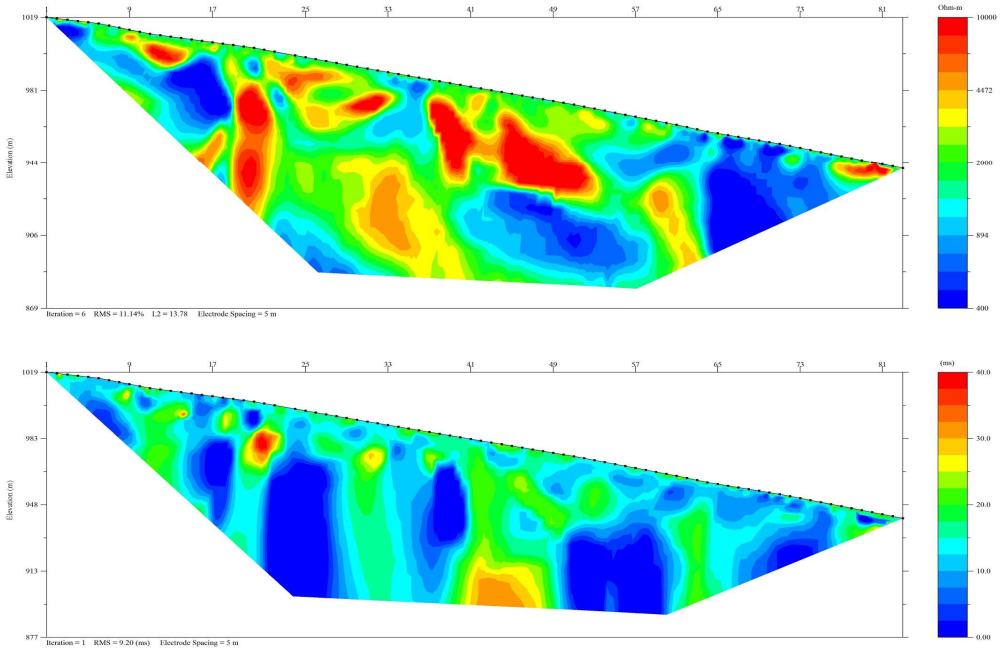

***Figure 34**: NOLIP17-32 sections. (**A**) Inverted resistivity (scale 400-10,000 Ohm-m). (**B**) Inverted IP (scale 0-40 ms).*

(A)

(B)

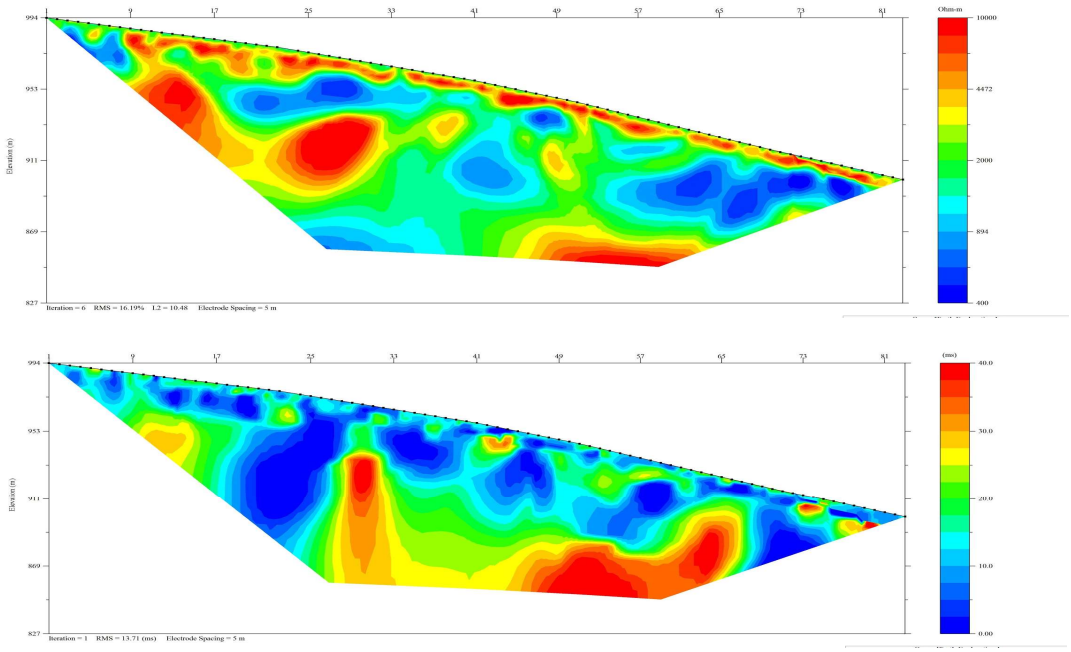

***Figure 35**: NOLIP17-33 sections. (**A**) Inverted resistivity (scale 400-10,000 Ohm-m). (**B**) Inverted IP (scale 0-40 ms).*

(A)

(B)

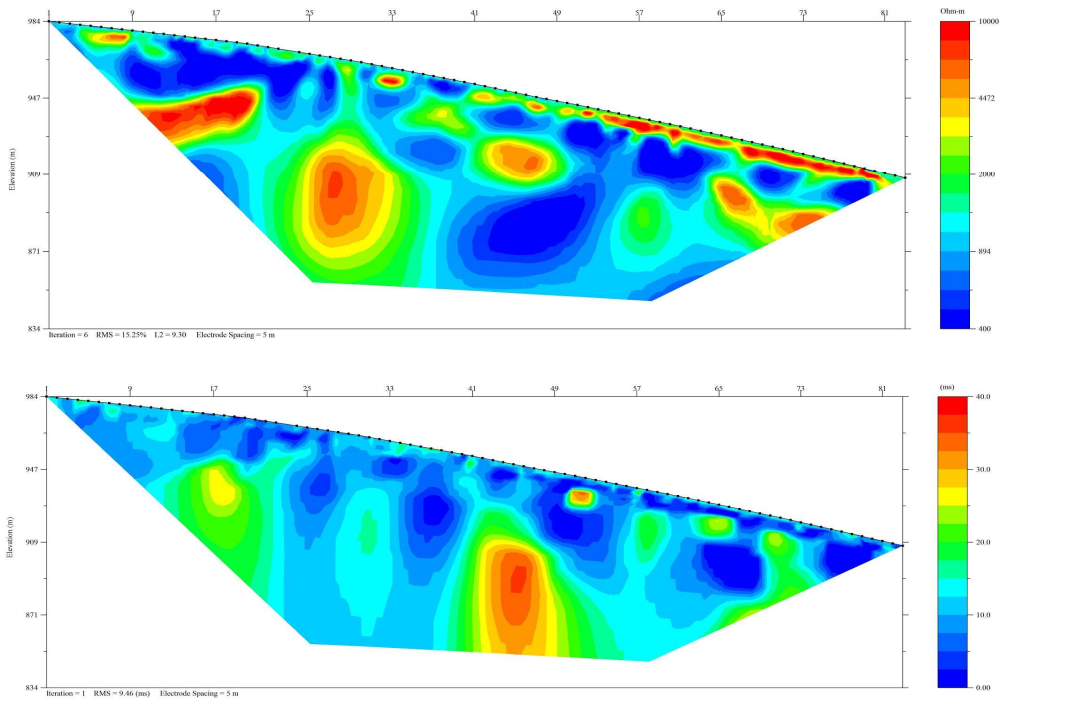

*Figure 36: NOLIP17-34 sections. (**A**) Inverted resistivity (scale 400-10,000 Ohm-m). (**B**) Inverted IP (scale 0-40 ms).*

7.3 Interpretation

The 2-D RES/IP surveys acquired in the Boucher area shows good qualitative correlation between anomalous resistivity and chargeability zones. The anomalies are sufficiently massive and smooth to give an indication of structure and mineralization within the grid area. To further constrain this interpretation, it is recommended that known geological and geochemical information is incorporated about the site. This will aid the interpreter to gain a better understanding of these anomalies and potentially aid them to identify geological structures and mineralized zones inherent to gold deposits.

Appendix A: Description of Files and File Structure

This section explains the file naming structure and data content for each project.

Each RES/IP traverse has a unique **Line ID** created by combining: (1) the three letter project code for the property or zone, (2) an IP or RES data designation, (3) the last two digits of the year the survey was read, and (4) an identifying number for the traverse within each property or zone.

> Example: ALBIP17-01, where ALB is the project code, IP is the type of data collected, 17 represents the year 2017, and 01 means that this is the first RES/IP dataset acquired on this property.

Each array dataset has a unique **Data File ID**. This ID is comprised by the date (yy-mm-dd), the first letter of the array type used (e.g. D for dipole-dipole or W for Wenner), and the number of times this array has been used that day.

> Example: 170813D1

File Structure and Content:

- DATA
  - └ Line ID
    - **Figures**
      - figures of merged data pseudosections and inversions
    - **GPS**
      - Contains the DGPS raw data
    - **Pictures**
      - Pictures along the line
    - **RAW**
      - **IP** (data with IP data-misfits removed)
      - **RES** (data with RES data-misfits removed)
      - unprocessed data from SuperSting unit
    - **XYZ**
      - Inverted data for RES and IP saved in XYZ format

Appendix B: SuperSting R1/IP technical specification

Measurement modes	Apparent resistivity, resistance, self potential (SP), induced polarization (IP), battery voltage
Measurement range	+/- 10V
Measuring resolution	Max 30 nV, depends on voltage level
Screen resolution	4 digits in engineering notation
Output current	1mA – 2 A continuous, measured to high accuracy
Output voltage	800 Vp-p, actual electrode voltage depends on transmitted current and ground resistivity
Output power	200 W
Input gain ranging	Automatic, always uses full dynamic range of receiver
Input impedance	>20 MΩ
SP compensation	Automatic cancellation of SP voltages during resistivity measurement. Constant and linearly varying SP cancels completely.
Type of IP measurement	Time domain chargability (M), six time slots measured and stored in memory
IP current transmission	ON+, OFF, ON-, OFF
IP time cycles	0.5, 1 , 2 , 4 and 8 seconds (combined resistivity/IP mode)
Measure cycles	Running average of measurement displayed after each cycle. Automatic cycle stop when reading errors fall below user set limit or user set max cycles are done.
Resistivity time cycles	Basic measure time is 0.4, 0.8, 1.2, 3.6, 7.2 or 14.4 seconds as selected by user via keyboard, autoranging and commutation adds about 1.4 s.
Signal processing	Continuous averaging after each complete cycle. Noise errors calculated and displayed as percentage of reading. Reading displayed as resistance (ΔV/I) and apparent resistivity (Ωm). Resistivity is calculated using user entered electrode array coordinates.
Noise suppression	Better than 100 dB at f>20 Hz Better than 120 dB at power line frequencies (16 2/3, 20, 50 and 60 Hz) for measure cycles of 1.2 s and above
Total accuracy	Better than 1% of reading in most cases (lab measurements). Field measurement accuracy depends on ground noise and resistivity. Instrument will calculate and display running estimate of measuring accuracy.
System calibration	Calibration is done digitally by the microprocessor based on correction values stored in memory.
Supported manual	Resistance, Schlumberger, Wenner, dipole-dipole, pole-dipole, pole-pole, SP-absolute, SP-gradient
Operating system	Stored in re-programmable flash memory. New version can be downloaded from our web site and stored in the flash memory.

Data storage	Full resolution reading average and error are stored along with user entered coordinates and time of day for each measurement. Storage is effected automatically in a job oriented file system
Data display	Apparent resistivity (Ohmmeter), injected current (mAmp) and measured voltage (mVolt) are displayed and stored in memory for each measurement
Memory capacity	The memory can store 24,468 measurements in Resistivity Mode and 14,966 measurements in combined Resistivity/IP Mode
Data transmission	RS-232C channel available to dump data from the instrument to a Windows type computer on user command.
Automatic multi-electrodes	The SuperSting is designed to run dipole-dipole, pole-dipole, pole-pole, Wenner and Schlumberger surveys including roll-along surveys completely automatic with the Swift Dual Mode Automatic Multi-electrode system (patent 6,404,203) or with switch box and passive cables. The SuperSting can run any other array by using user programmed command files. These files are ASCII files and can be created using a regular text editor. The command files are downloaded to the SuperSting RAM memory and can at any time be recalled and run. Therefore there is no need for a fragile computer in the field.
Manual measurements	The instrument has four banana pole screws for connecting current and potential electrodes during manual measurments
User controls	20 key tactile, weather proof keyboard with alpha numeric entry keys and function keys. On/off switch. Measure button. LCD night light switch (push to light).
Display	Graphics LCD display (16 lines x 30 characters) with night light.
Power supply, field	12V or 2x12 V DC external power (one or two 12 V batteries), connector on front panel.
Power supply, office	DC power supply
Operating time	Depends on survey conditions and size of battery used. Internal circuitry in auto mode adjusts current to save energy
Operating temperature	-5 to +50ºC
Weight	10.9 kg (24 lb.)
Dimensions	Width 184 mm (7.25"), length 406 mm (16") and height 273 mm (10.75”)

Appendix C: Extended Dipole-Dipole Array

The extended dipole-dipole array provides extended data coverage of the standard dipole-dipole array. The electrode configuration for dipole-dipole is shown below, where the current electrodes (A and B) and potential electrodes (M and N) are equivalently spaced by “a”, and separated by a factor “n” times the spacing “a”. A measurement of apparent resistivity can be calculated using the equation below the figure, where V = potential difference (V), I = current (Amp), and ρ_A = apparent resistivity (Ohm-m).

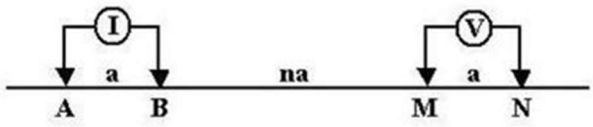

$$\rho_A = \frac{V}{I}\pi\, a\, n(n+1)(n+2).$$

Penetration depth of the extended dipole-dipole array (measurement locations shown below) is approximately 14 times the electrode spacing, which is equivalent to 70m using 5m electrode spacing, but is also dependent on: (1) the actual distribution of subsurface resistivity, and (2) the best achievable contact resistance values between the electrodes and the ground. The figure below shows the measurement locations (in pseudo depth) for an extended dipole-dipole array using 84 surface electrodes.

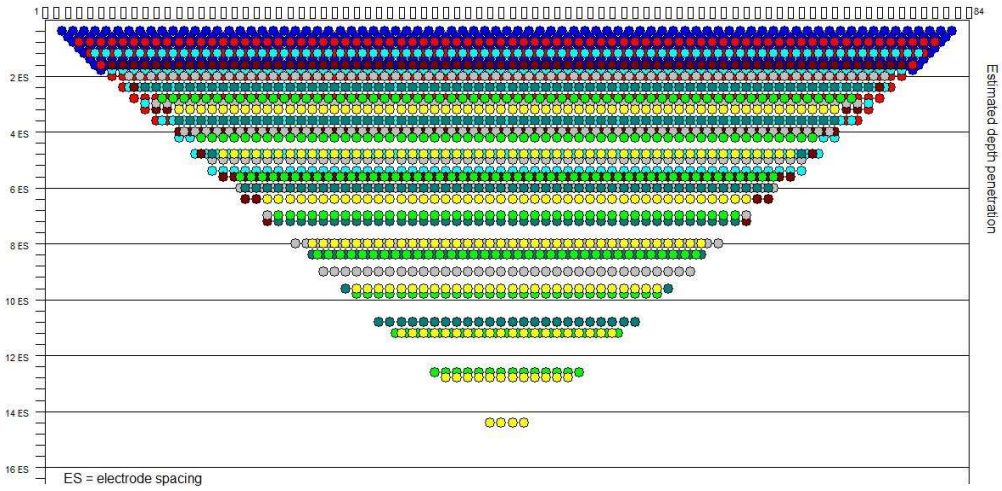

Appendix D: Data Misfit Crossplots

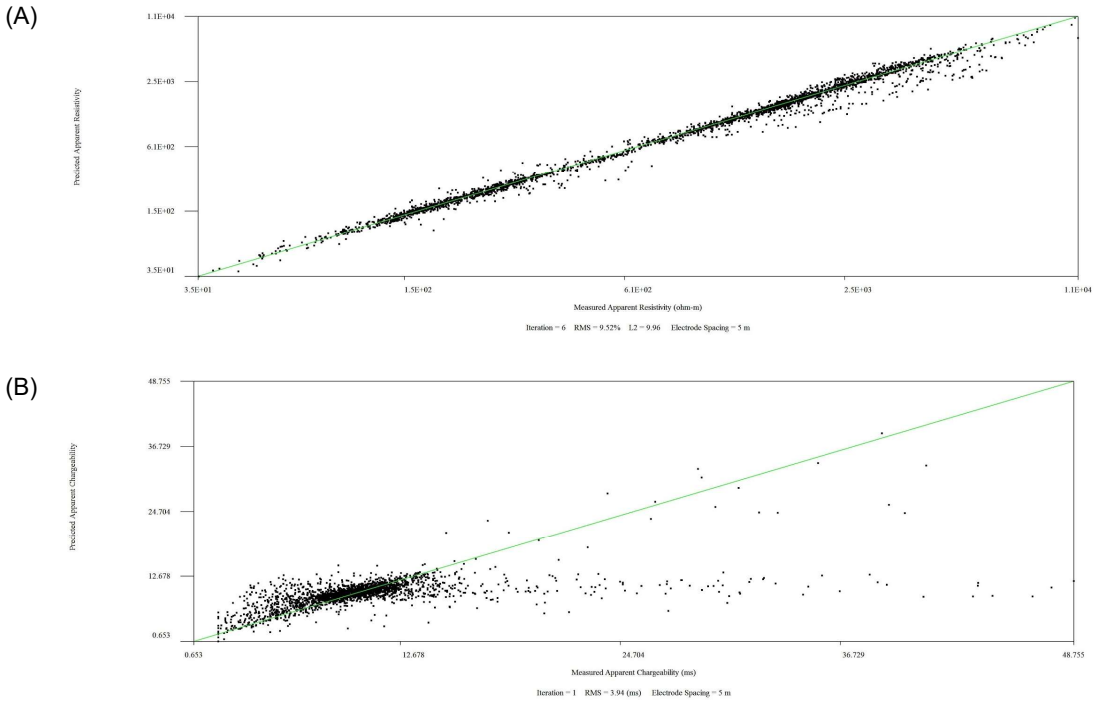

***Figure D-1**: NOLIP17-01 data misfit crossplots. (**A**) Measured vs. predicted apparent resistivity (Ohm-m). (**B**) Measured vs. predicted chargeability (ms).*

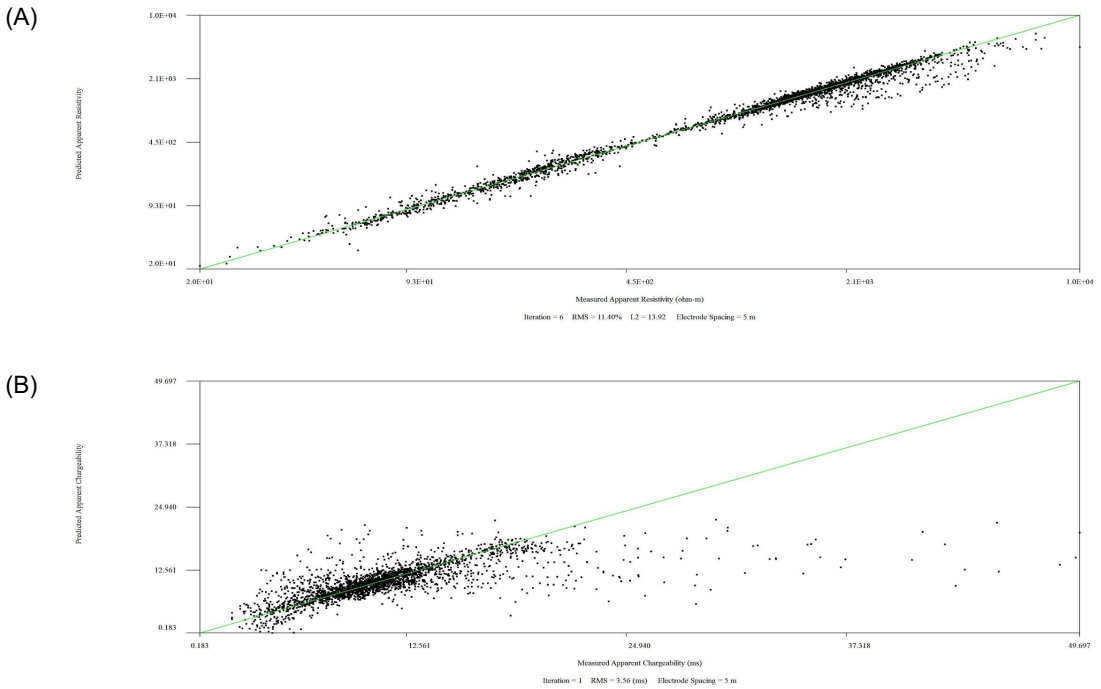

***Figure D-2**: NOLIP17-02 data misfit crossplots. (**A**) Measured vs. predicted apparent resistivity (Ohm-m). (**B**) Measured vs. predicted chargeability (ms).*

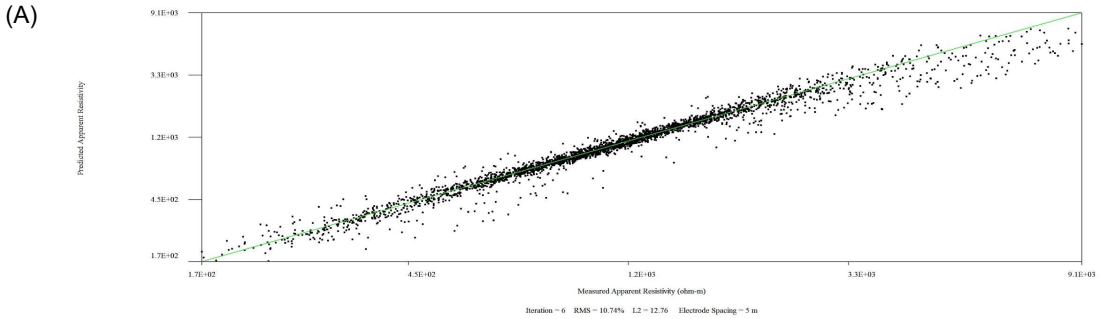

(B)

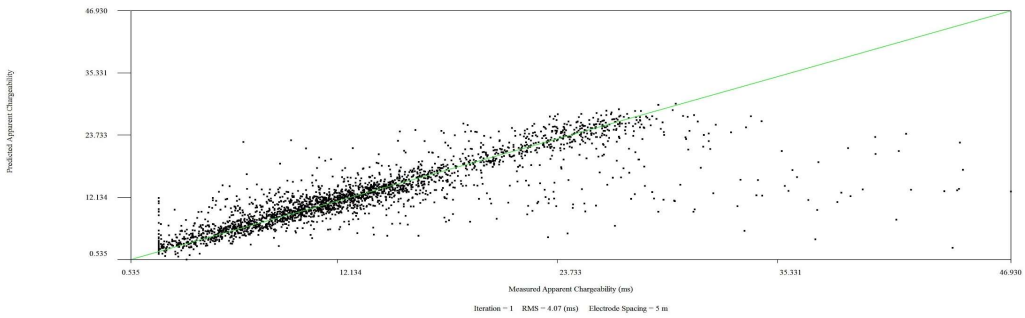

***Figure D-3**: NOLIP17-03 data misfit crossplots. (**A**) Measured vs. predicted apparent resistivity (Ohm-m). (**B**) Measured vs. predicted chargeability (ms).*

(A)

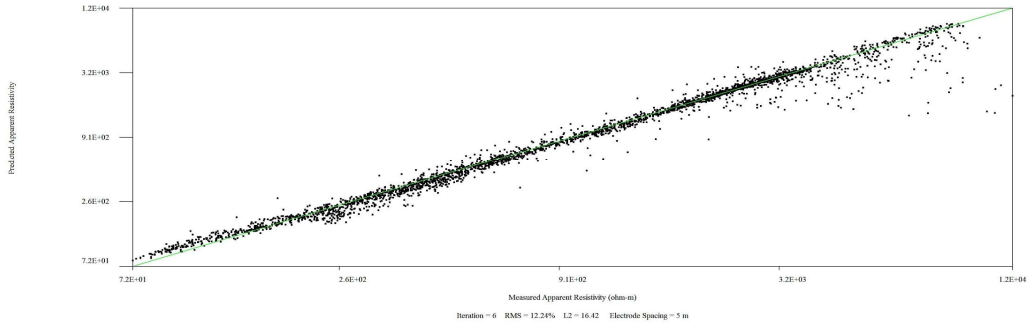

(B)

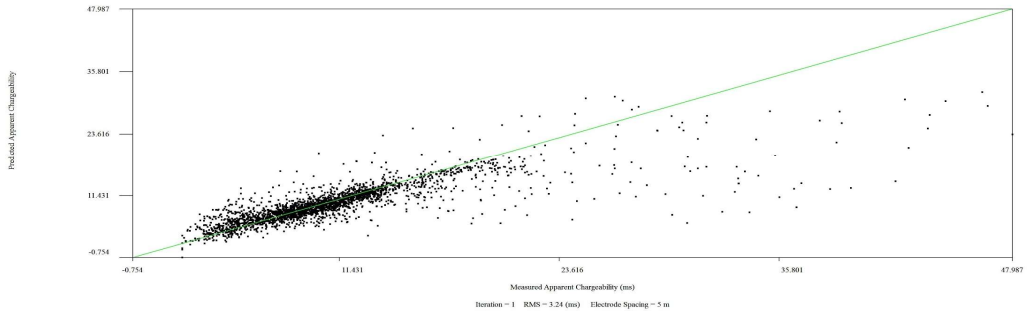

***Figure D-4**: NOLIP17-04 data misfit crossplots. (**A**) Measured vs. predicted apparent resistivity (Ohm-m). (**B**) Measured vs. predicted chargeability (ms).*

(A)

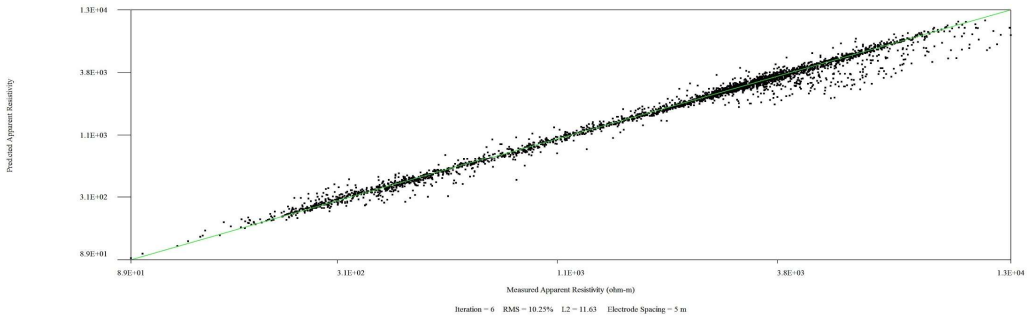

(B)

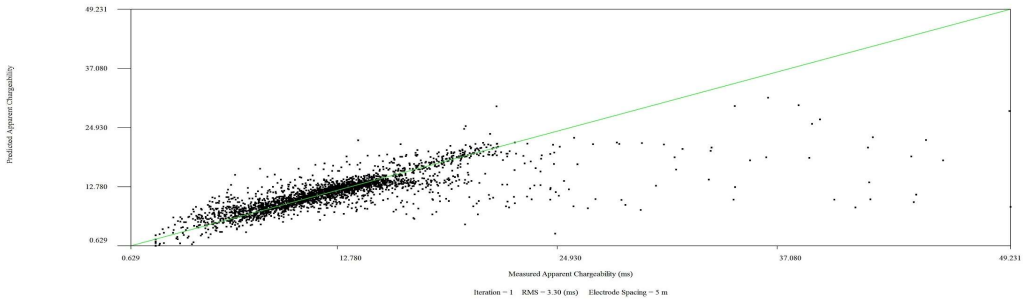

***Figure D-5**: NOLIP17-05 data misfit crossplots. (**A**) Measured vs. predicted apparent resistivity (Ohm-m). (**B**) Measured vs. predicted chargeability (ms).*

(A)

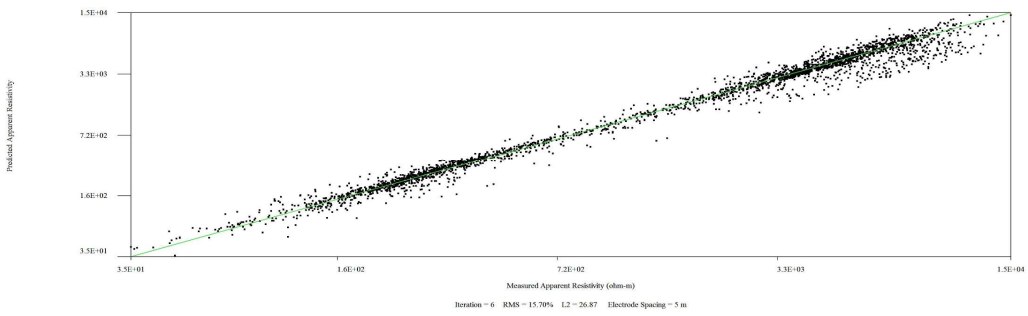

(B)

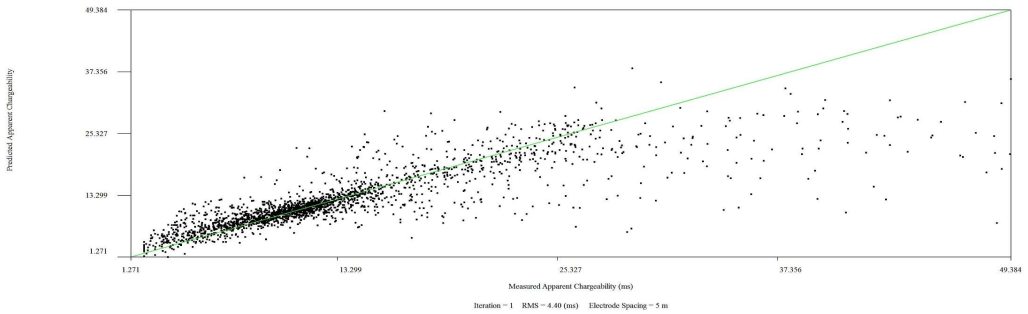

***Figure D-6**: NOLIP17-06 data misfit crossplots. (**A**) Measured vs. predicted apparent resistivity (Ohm-m). (**B**) Measured vs. predicted chargeability (ms).*

(A)

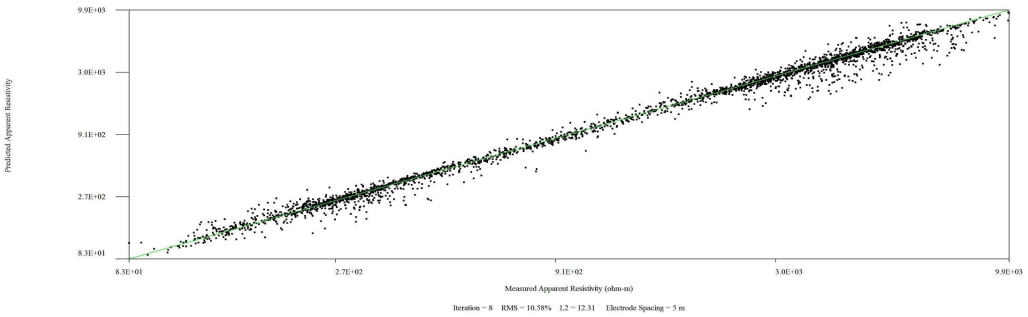

(B)

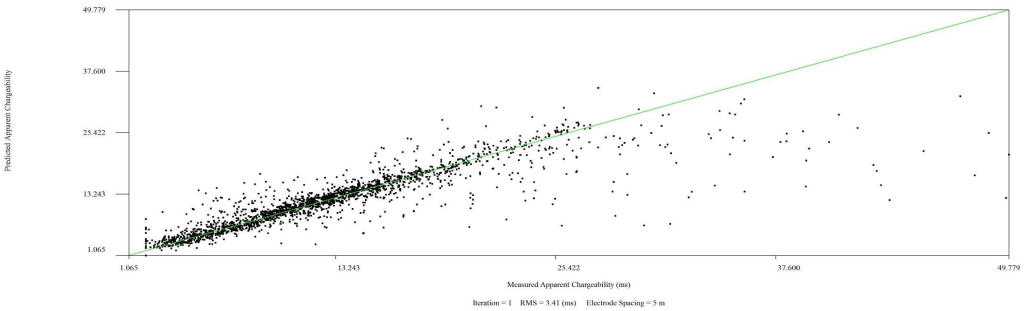

***Figure D-7**: NOLIP17-07 data misfit crossplots. (**A**) Measured vs. predicted apparent resistivity (Ohm-m). (**B**) Measured vs. predicted chargeability (ms).*

(A)

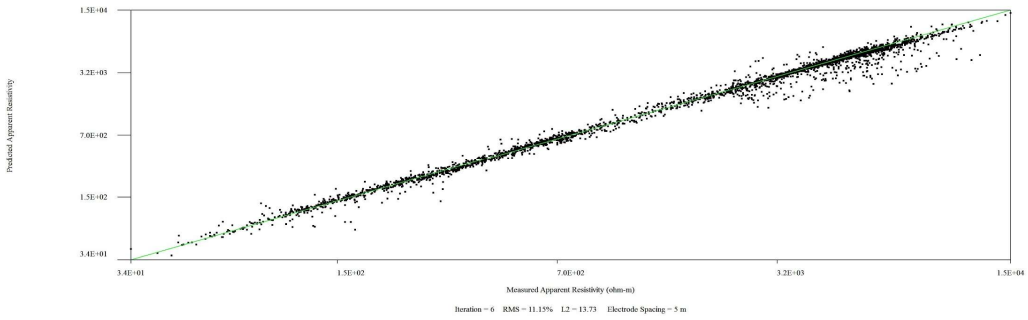

(B)

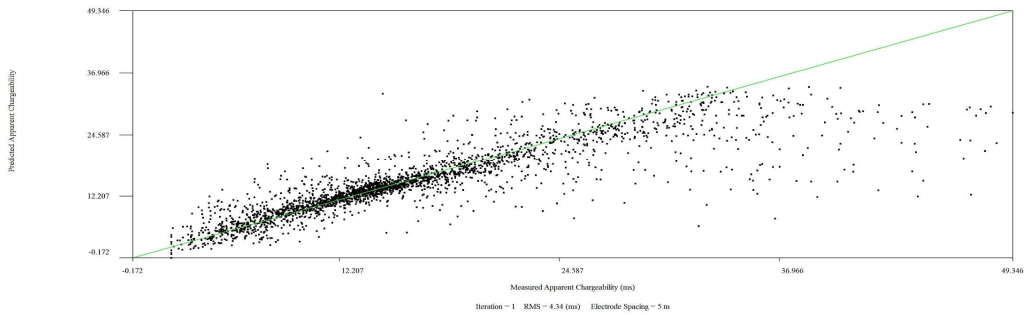

***Figure D-8**: NOLIP17-08 data misfit crossplots. (**A**) Measured vs. predicted apparent resistivity (Ohm-m). (**B**) Measured vs. predicted chargeability (ms).*

(A)

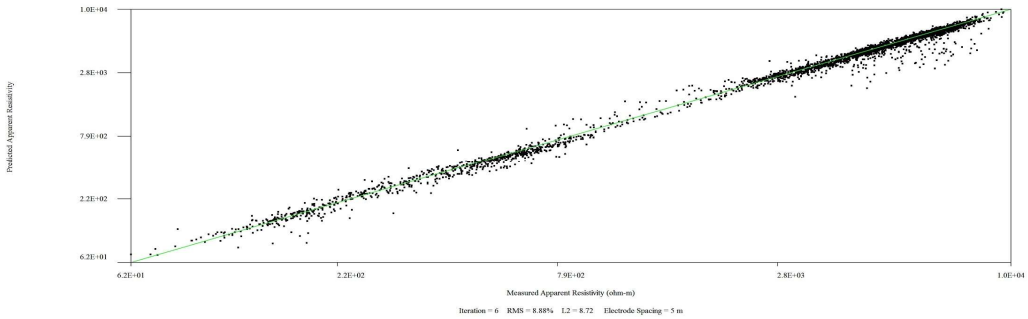

(B)

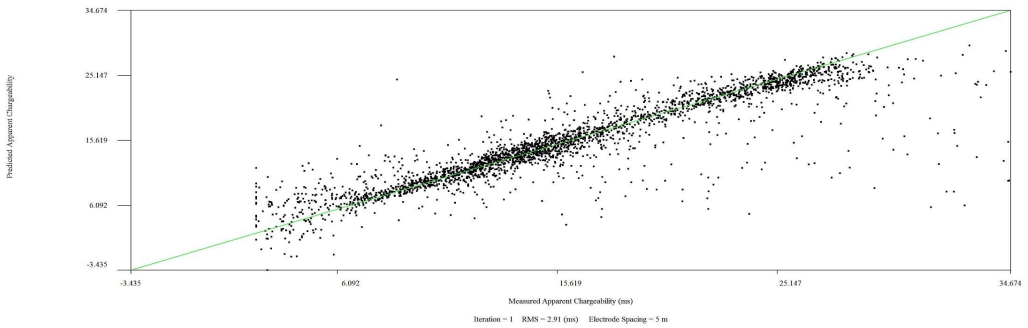

***Figure D-9**: NOLIP17-09 data misfit crossplots. (**A**) Measured vs. predicted apparent resistivity (Ohm-m). (**B**) Measured vs. predicted chargeability (ms).*

(A)

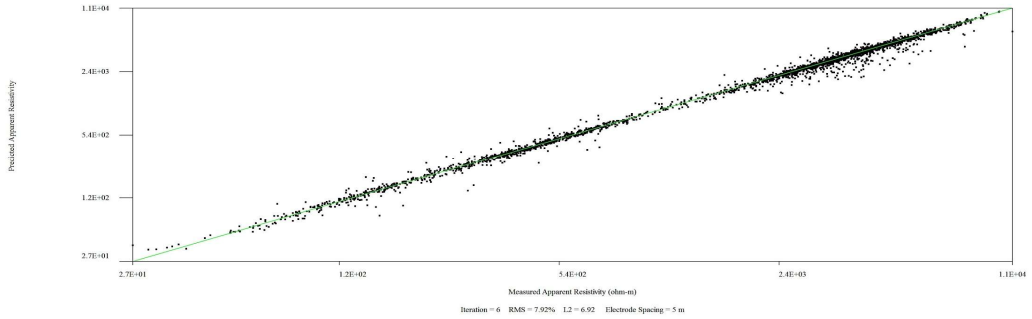

(B)

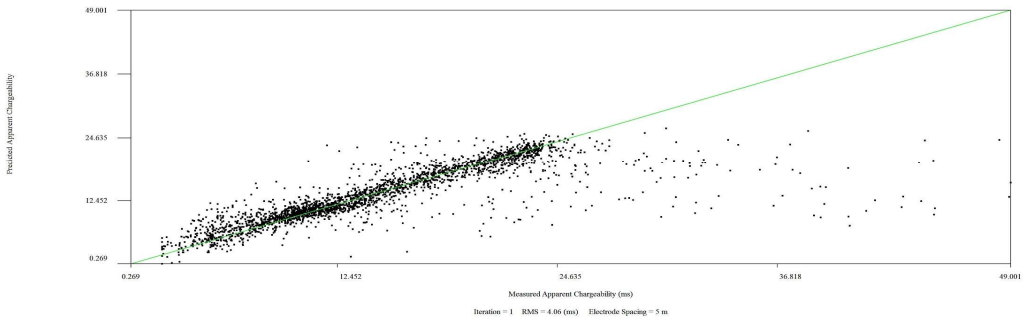

***Figure D-10**: NOLIP17-10 data misfit crossplots. (**A**) Measured vs. predicted apparent resistivity (Ohm-m). (**B**) Measured vs. predicted chargeability (ms).*

(A)

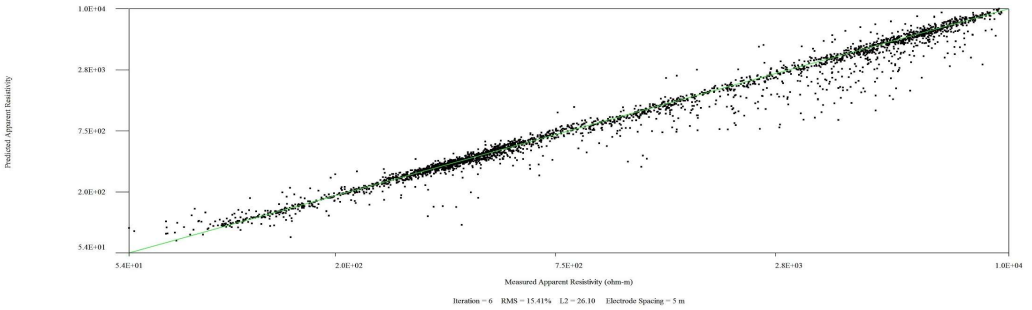

(B)

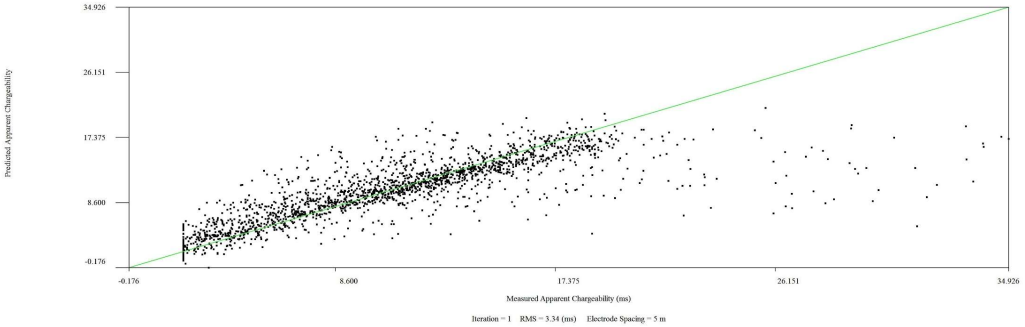

***Figure D-11**: NOLIP17-11 data misfit crossplots. (**A**) Measured vs. predicted apparent resistivity (Ohm-m). (**B**) Measured vs. predicted chargeability (ms).*

(A)

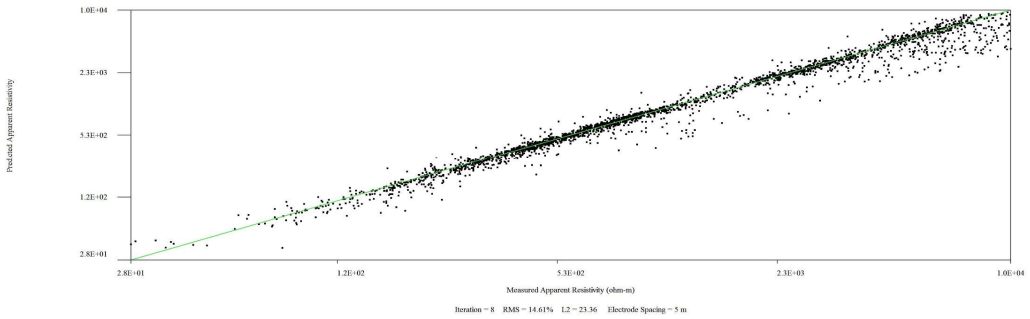

(B)

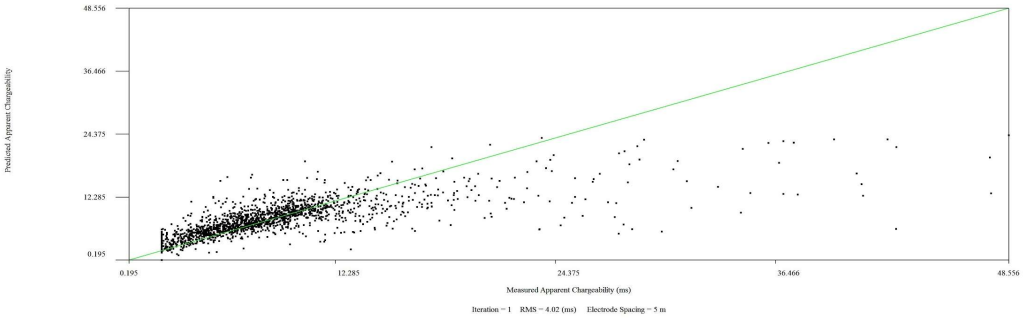

***Figure D-12**: NOLIP17-12 data misfit crossplots. (**A**) Measured vs. predicted apparent resistivity (Ohm-m). (**B**) Measured vs. predicted chargeability (ms).*

(A)

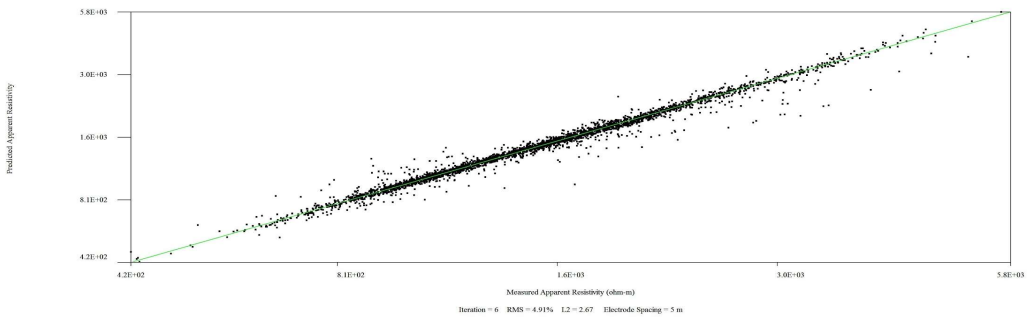

(B)

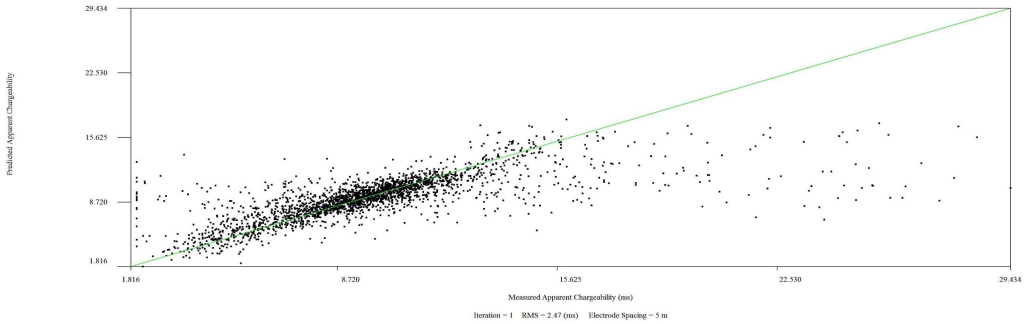

***Figure D-13**: NOLIP17-13 data misfit crossplots. (**A**) Measured vs. predicted apparent resistivity (Ohm-m). (**B**) Measured vs. predicted chargeability (ms).*

(A)

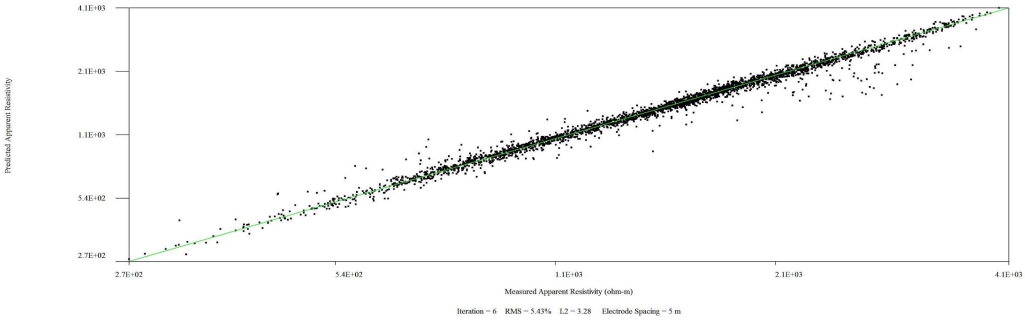

(B)

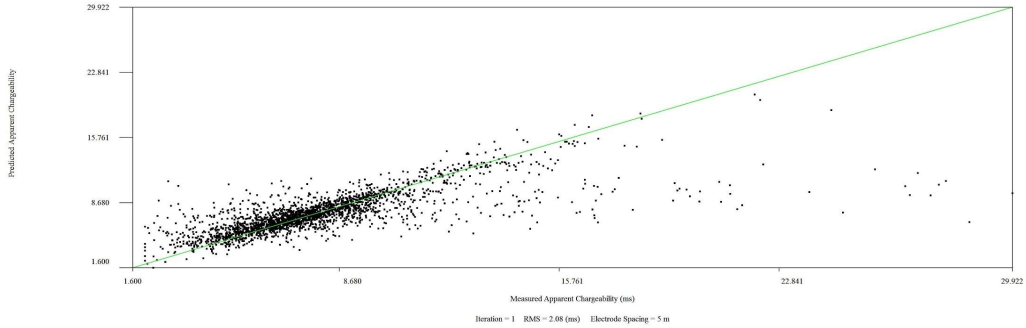

***Figure D-14**: NOLIP17-14 data misfit crossplots. (**A**) Measured vs. predicted apparent resistivity (Ohm-m). (**B**) Measured vs. predicted chargeability (ms).*

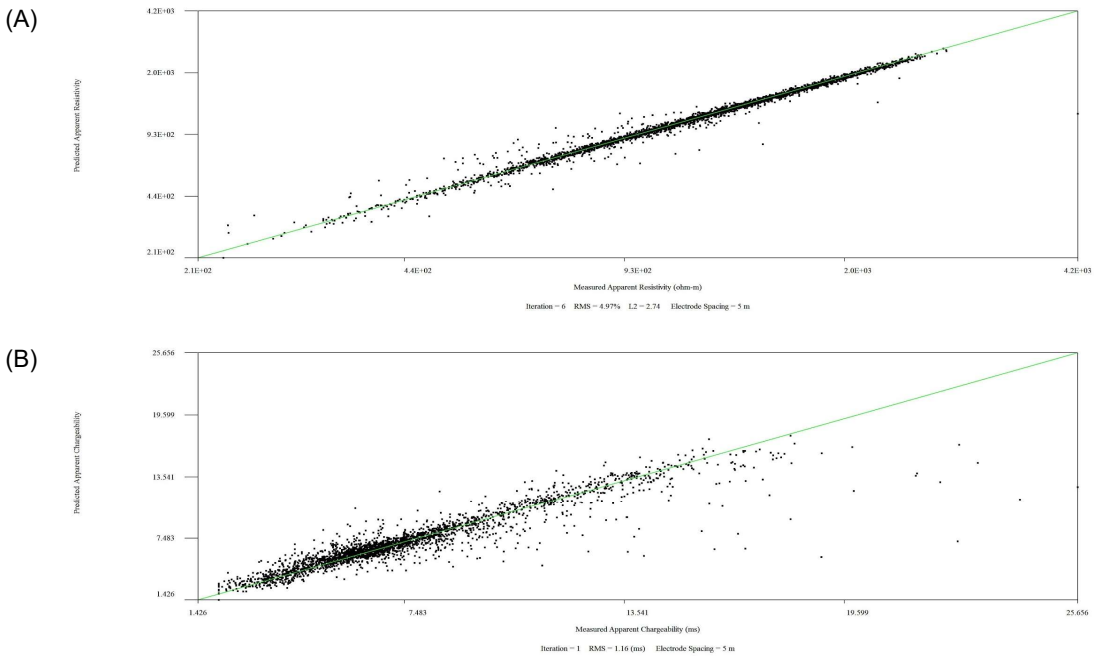

***Figure D-15**: NOLIP17-15 data misfit crossplots. (**A**) Measured vs. predicted apparent resistivity (Ohm-m). (**B**) Measured vs. predicted chargeability (ms).*

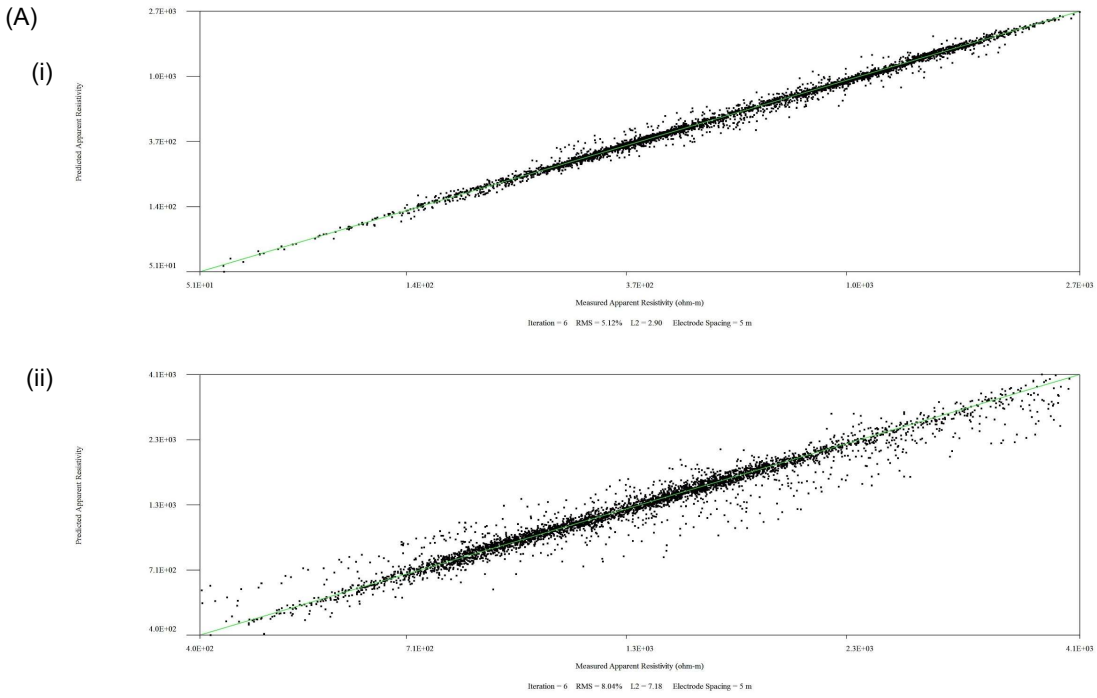

(iii)

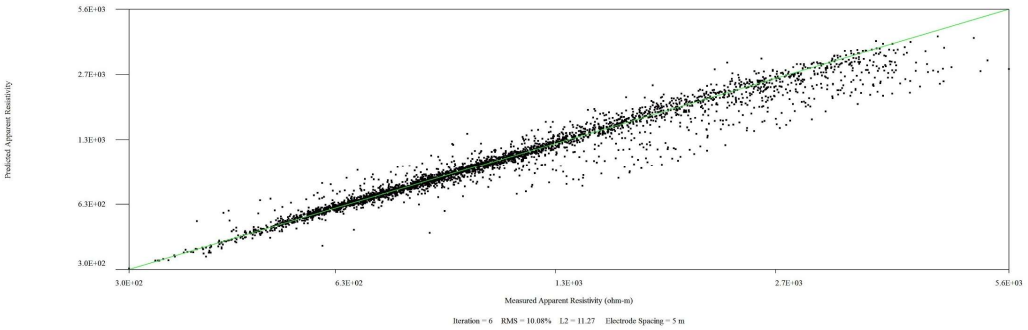

(B)

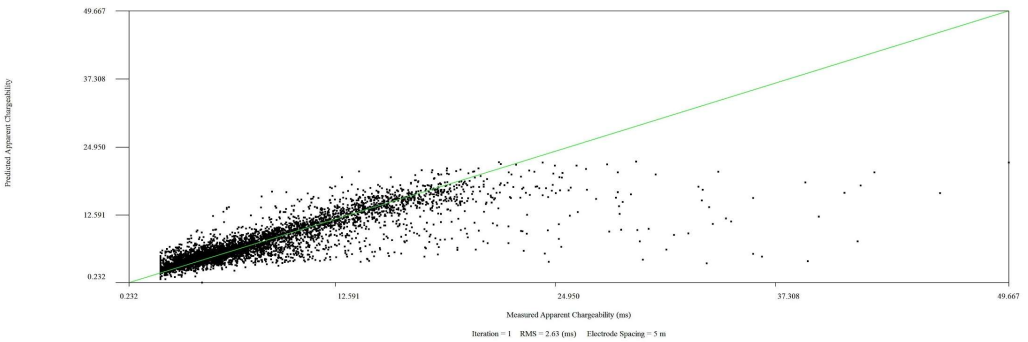

***Figure D-16**: NOLIP17-16 data misfit crossplots. (**A**) Measured vs. predicted apparent resistivity (Ohm-m) for (i) electrodes 1-100, (ii) electrodes 50-150, and (iii) electrodes 100-193. (**B**) Measured vs. predicted chargeability (ms) for electrodes 1-193.*

(A)

(i)

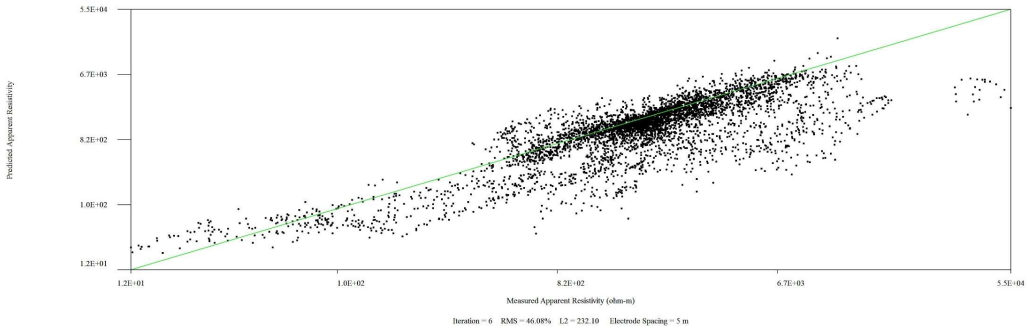

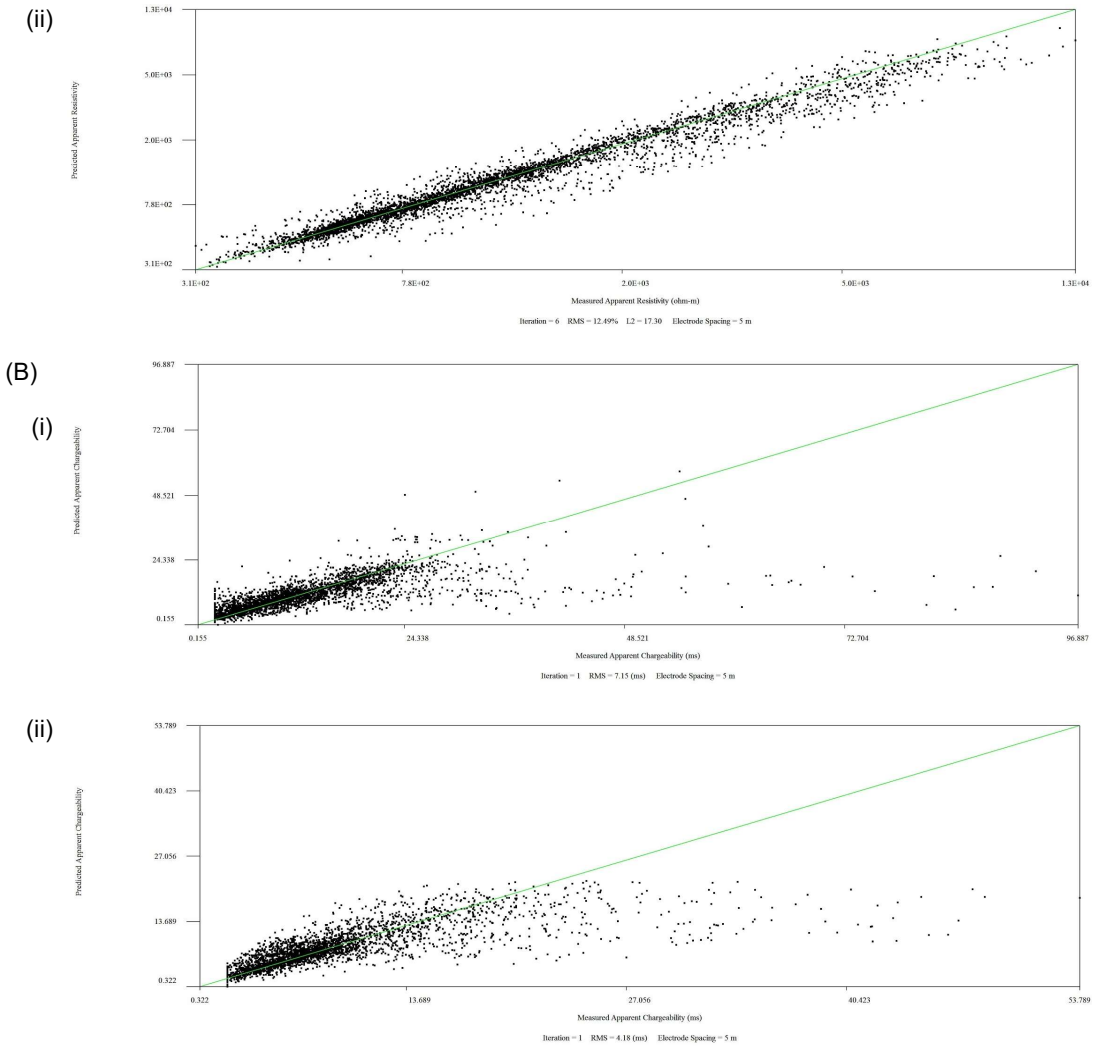

***Figure D-17**: NOLIP17-17 data misfit crossplots. (**A**) Measured vs. predicted apparent resistivity (Ohm-m) for (i) electrodes 1-120, and (ii) electrodes 60-183. (**B**) Measured vs. predicted chargeability (ms) for (i) electrodes 1-120, and (ii) electrodes 60-183.*

(A)

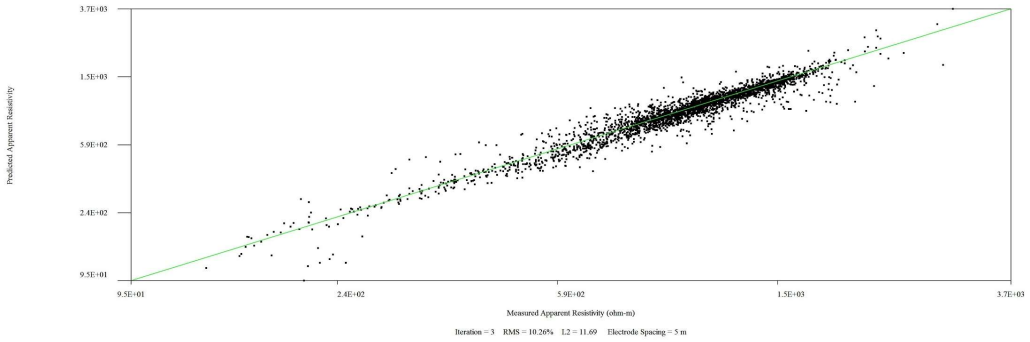

(B)

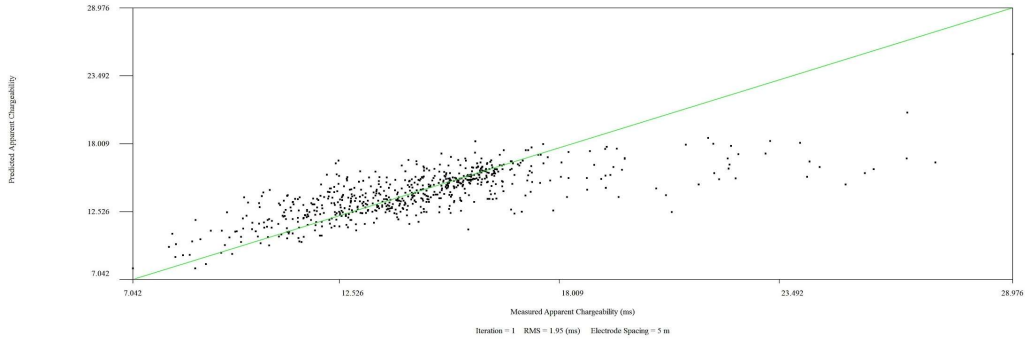

***Figure D-18**: NOLIP17-18 data misfit crossplots. (**A**) Measured vs. predicted apparent resistivity (Ohm-m). (**B**) Measured vs. predicted chargeability (ms).*

(A)

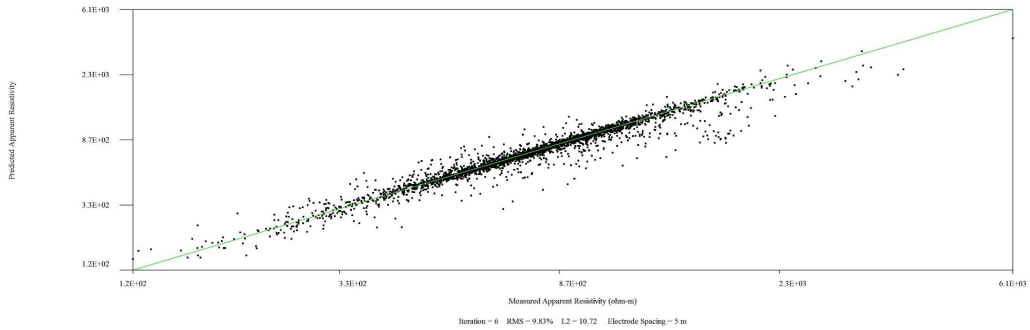

***Figure D-19**: NOLIP17-19 data misfit crossplots. (**A**) Measured vs. predicted apparent resistivity (Ohm-m).*

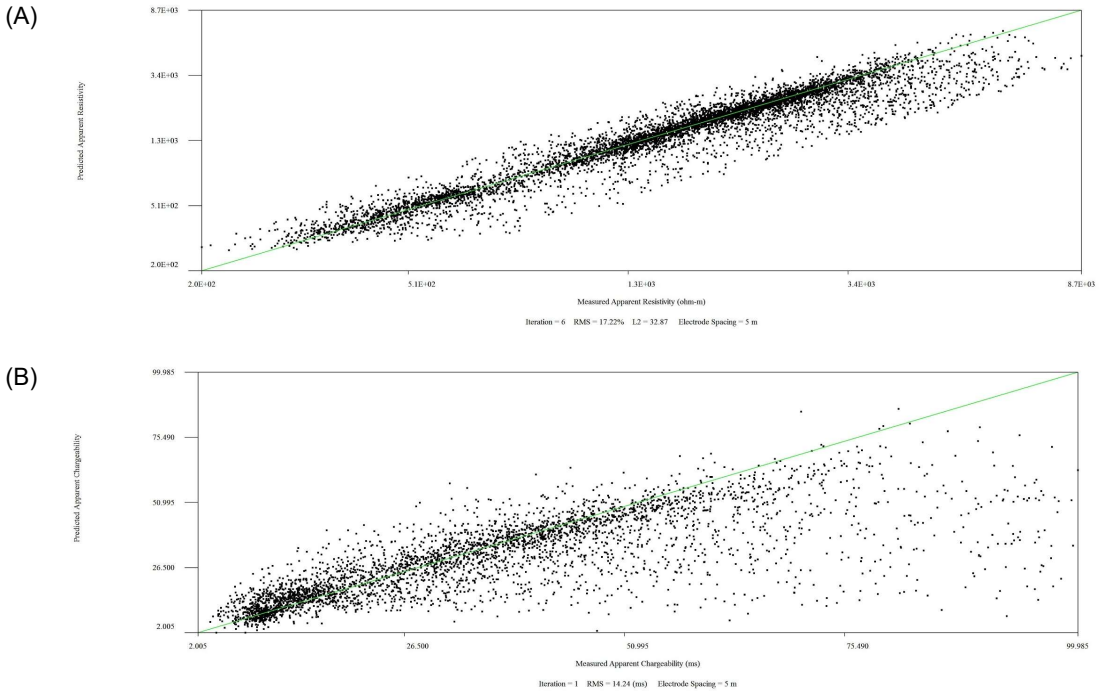

***Figure D-20**: NOLIP17-20 data misfit crossplots. (**A**) Measured vs. predicted apparent resistivity (Ohm-m). (**B**) Measured vs. predicted chargeability (ms).*

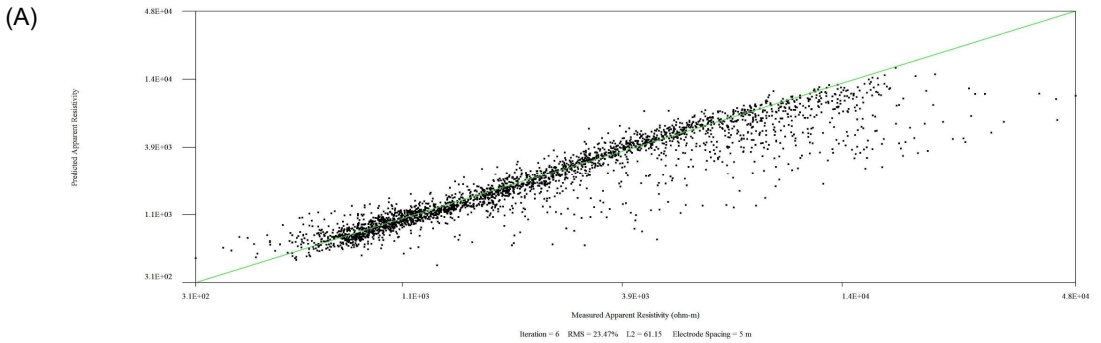

***Figure D-21**: NOLIP17-21 data misfit crossplots. (**A**) Measured vs. predicted apparent resistivity (Ohm-m).*

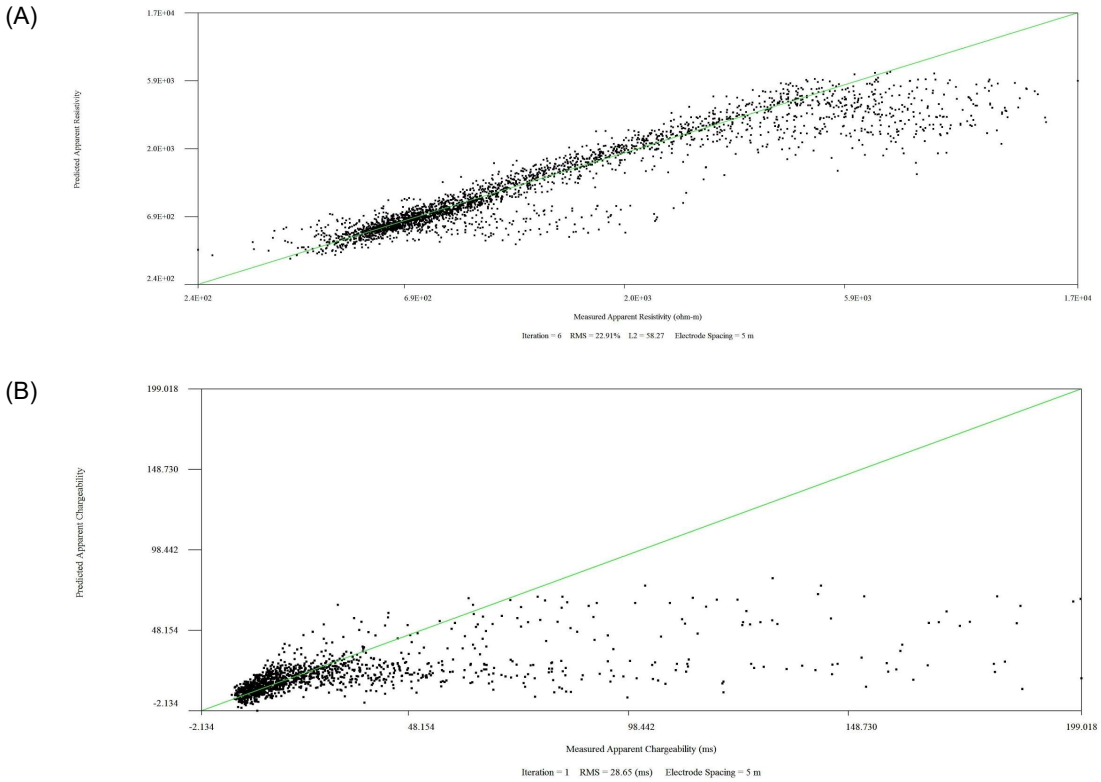

***Figure D-22**: NOLIP17-22 data misfit crossplots. (**A**) Measured vs. predicted apparent resistivity (Ohm-m). (**B**) Measured vs. predicted chargeability (ms).*

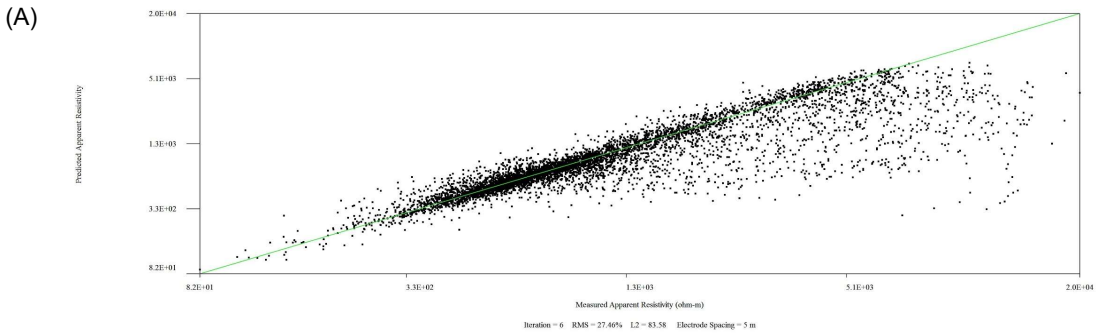

***Figure D-23**: NOLIP17-23 data misfit crossplot. (**A**) Measured vs. predicted apparent resistivity (Ohm-m).*

(A)

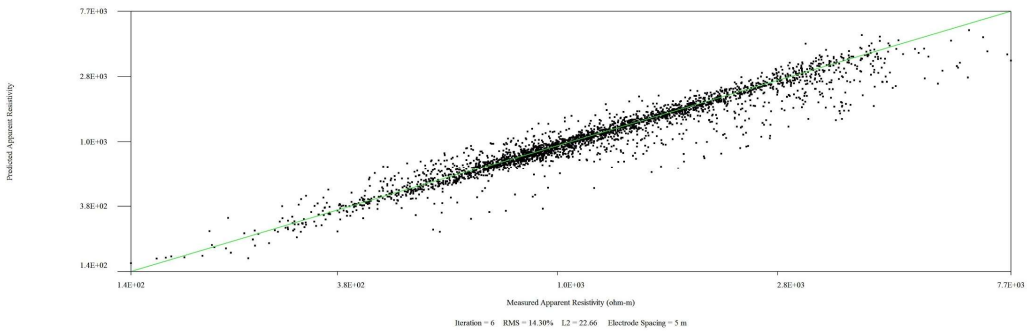

***Figure D-24**: NOLIP17-24 data misfit crossplot. (**A**) Measured vs. predicted apparent resistivity (Ohm-m).*

(A)

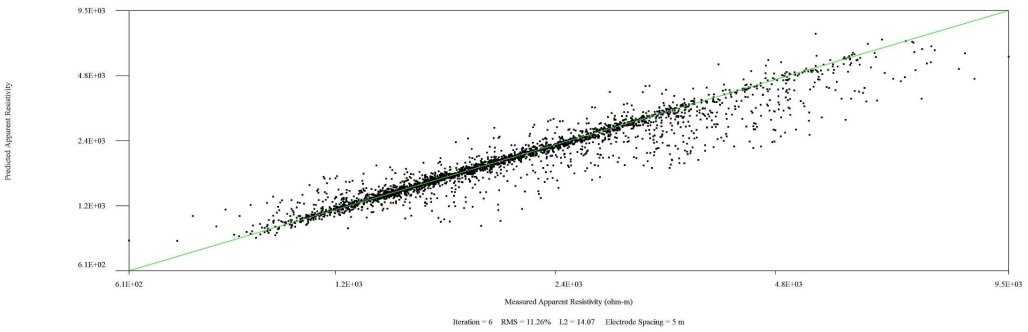

(B)

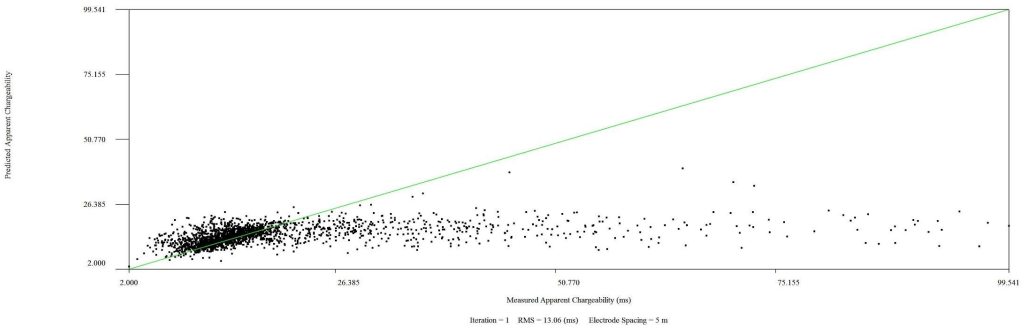

***Figure D-25**: BOUIP17-25 data misfit crossplots. (**A**) Measured vs. predicted apparent resistivity (Ohm-m). (**B**) Measured vs. predicted chargeability (ms).*

(A)

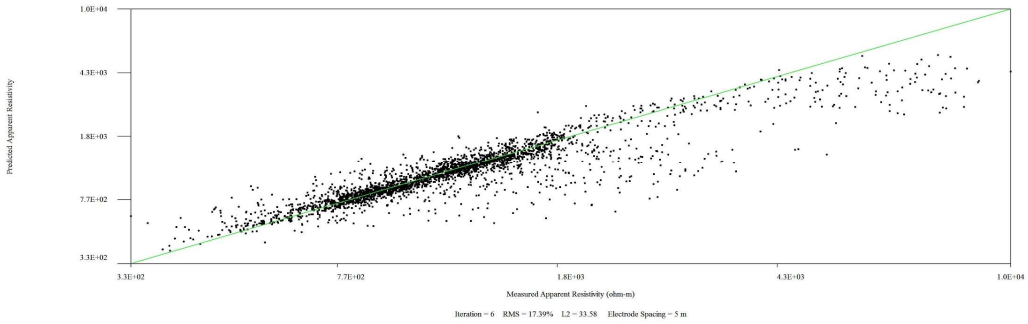

(B)

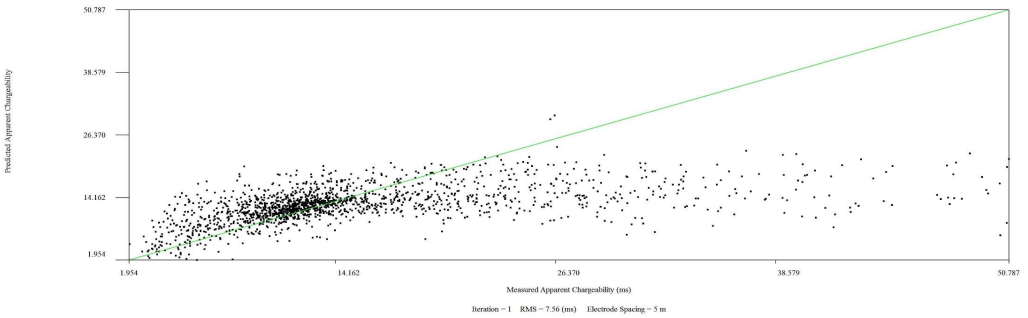

***Figure D-26**: BOUIP17-27 data misfit crossplots. (**A**) Measured vs. predicted apparent resistivity (Ohm-m). (**B**) Measured vs. predicted chargeability (ms).*

(A)

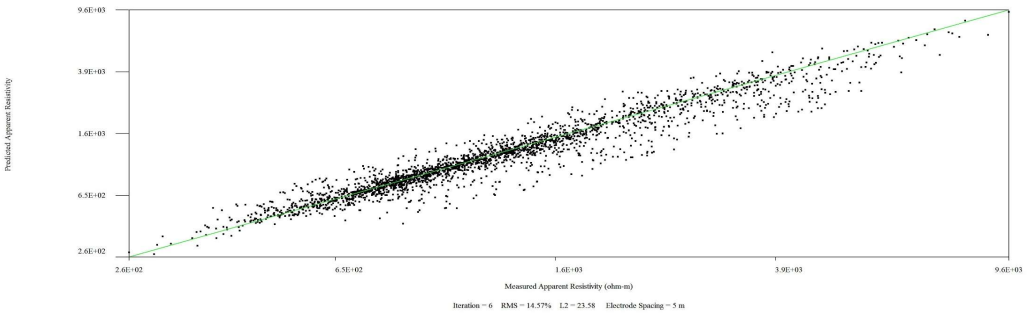

(B)

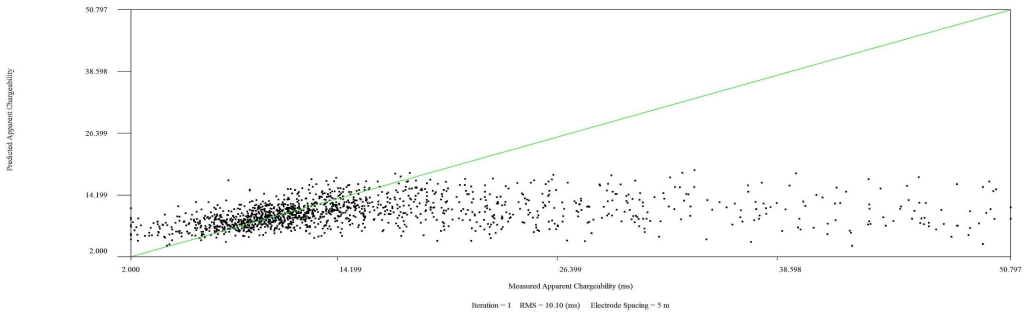

***Figure D-27**: BOUIP17-28 data misfit crossplots. (**A**) Measured vs. predicted apparent resistivity (Ohm-m). (**B**) Measured vs. predicted chargeability (ms).*

(A)

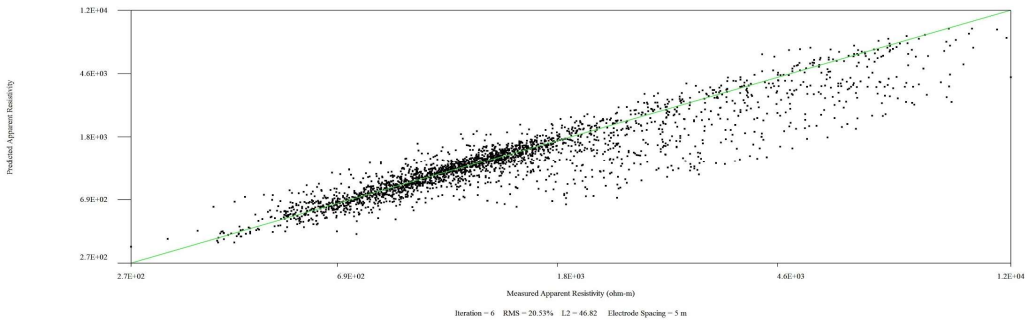

(B)

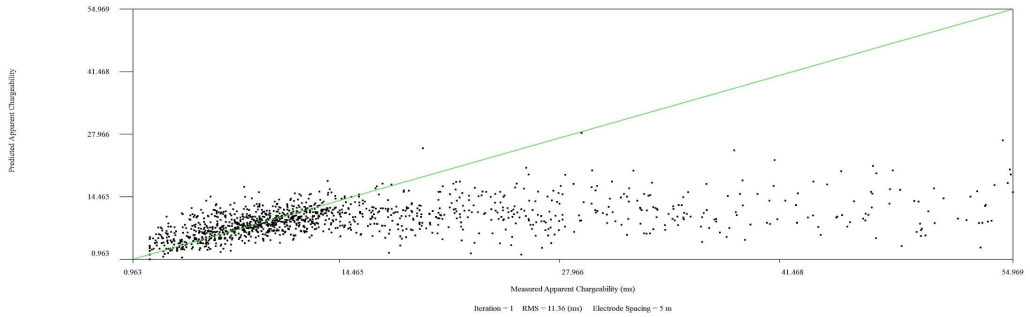

***Figure D-28**: BOUIP17-30 data misfit crossplots. (**A**) Measured vs. predicted apparent resistivity (Ohm-m). (**B**) Measured vs. predicted chargeability (ms).*

(A)

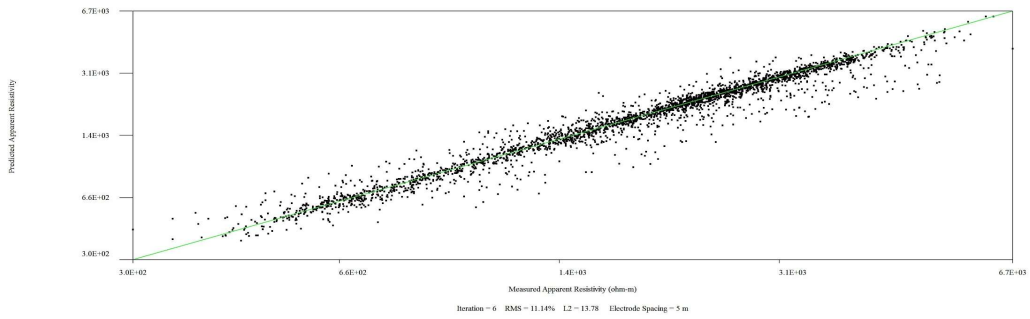

(B)

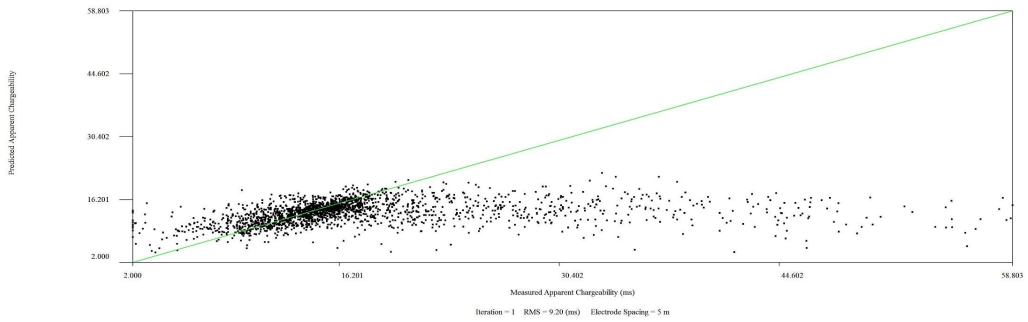

***Figure D-29**: BOUIP17-32 data misfit crossplots. (**A**) Measured vs. predicted apparent resistivity (Ohm-m). (**B**) Measured vs. predicted chargeability (ms).*

(A)

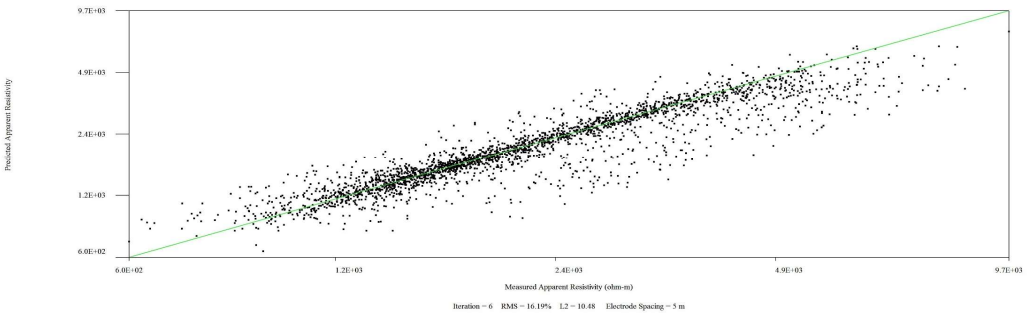

(B)

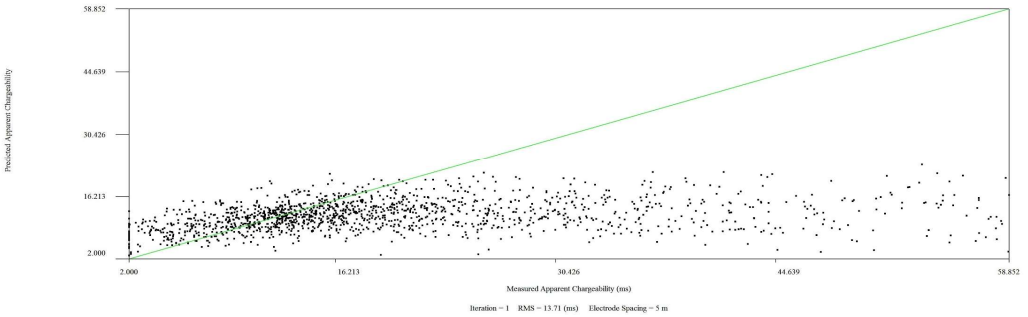

***Figure D-30**: BOUIP17-33 data misfit crossplots. (**A**) Measured vs. predicted apparent resistivity (Ohm-m). (**B**) Measured vs. predicted chargeability (ms).*

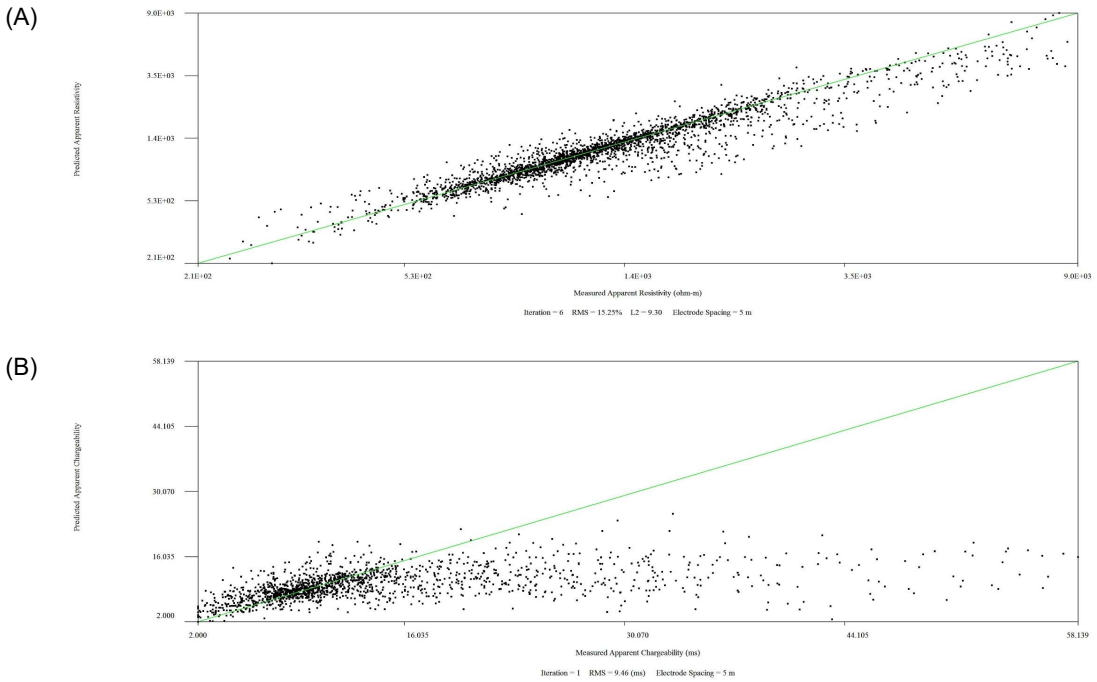

***Figure D-31**: BOUIP17-34 data misfit crossplots. (**A**) Measured vs. predicted apparent resistivity (Ohm-m). (**B**) Measured vs. predicted chargeability (ms).*